
SpecSphere: Dual-Pass Spectral–Spatial Graph Neural Networks with Certified Robustness

Yoonhyuk Choi

Samsung SDS

Seoul, South Korea

chldbsgur123@gmail.com

Chong-Kwon Kim*

KENTECH

Naju, South Korea

ckim@kentech.ac.kr

Abstract

We introduce SpecSphere, the first dual-pass spectral–spatial GNN that certifies every prediction against both ℓ_0 edge flips and ℓ_∞ feature perturbations, adapts to the full homophily–heterophily spectrum, and surpasses the expressive power of 1-Weisfeiler–Lehman while retaining linear-time complexity. Our model couples a Chebyshev-polynomial spectral branch with an attention-gated spatial branch and fuses their representations through a lightweight MLP trained in a cooperative–adversarial min–max game. We further establish (i) a uniform Chebyshev approximation theorem, (ii) minimax-optimal risk across the homophily–heterophily spectrum, (iii) closed-form robustness certificates, and (iv) universal approximation strictly beyond 1-WL. SpecSphere achieves state-of-the-art node-classification accuracy and delivers tighter certified robustness guarantees on real-world benchmarks. These results demonstrate that high expressivity, heterophily adaptation, and provable robustness can coexist within a single, scalable architecture.

1 Introduction

Graph neural networks (GNNs) have become the backbone of modern systems for node classification [25], link prediction [54], and graph-level reasoning [28]. Most popular architectures implement Laplacian-based filtering or neighborhood message passing, implicitly enforcing a low-pass prior that assumes homophily, where adjacent nodes share labels and features [39].

However, many real-world graphs exhibit heterophily in which connected nodes belong to different classes or display contrasting attributes [41; 48]. Under these conditions, the inherent low-pass bias of standard graph convolutions smooths away critical high-frequency signals [52]. Without explicit priors, even advanced spectral filters struggle to recover the lost discriminative details [14]. To address this, recent hybrid architectures have introduced mechanisms to reorder or decouple message pathways, preserving high-frequency components on heterophilic benchmarks [16].

Robustness constitutes a second critical challenge. Minor structure edits ℓ_0 (e.g., a handful of edge flips) can invert predictions [34], while small ℓ_∞ perturbations on node features suffice to fool classifiers [23]. Although adversarial training improves empirical defense, it can overfit to a single threat model and remains brittle under adaptive attacks [18]. Certified defenses seek formal worst-case guarantees, but existing certificates are largely restricted to single-branch architectures [61].

Finally, expressivity limits standard message-passing GNNs to the power of the one-dimensional Weisfeiler–Lehman (1-WL) test. Extensions inject random features [15], aggregate higher-order substructures [38; 1], or adapt spectral responses [2; 14]. Nonetheless, no prior work unifies high expressivity with node-wise homophily adaptation and a provable, dual-norm robustness guarantee.

* corresponding author

Model	Architecture	Certification	Heterophily	Expressivity
Certified GNN [47]	Single	Certified ℓ_0	No	No
ACM-GNN [33]	Hybrid	No	Adaptive	Standard
EvenNet [29]	Spectral	Certified ℓ_∞	Static	Standard
GARNET [12]	Spectral	Empirical	Adaptive	Standard
S ² GNN [16]	Hybrid	No	No	> 1-WL
TFE-GNN [14]	Spectral	No	Adaptive	Standard
PCNet [30]	Dual	No	Adaptive	Standard
SPCNet [31]	Dual	Partial	Adaptive	Standard
SpecSphere (ours)	Dual	Certified (ℓ_0, ℓ_∞)	Adaptive	> 1-WL

Table 1: Comprehensive comparison of spectral–spatial and robustness-aware GNNs. “Architecture” distinguishes single-pass (Spectral or Spatial), hybrid (one filter type), and dual-pass (both). “Certification” indicates provable bounds where available. More baselines are introduced in **Appendix A**

We close this gap with SpecSphere. Our certificate separately bounds the Lipschitz constants of a Chebyshev-based spectral branch and an attention-gated spatial branch, then propagates these bounds through a fusion MLP. Training is framed as a cooperative–adversarial game: alternating projected-gradient steps for the attacker and stochastic-gradient updates for the network converge to an $\mathcal{O}(T^{-1/2})$ stationary point under standard smoothness and bounded-gap assumptions.

Direct comparison to existing methods. Table 1 shows that SpecSphere is the first dual-pass spectral–spatial GNN to offer both certified (ℓ_0, ℓ_∞) robustness and per-node heterophily adaptation. Unlike prior dual-pass designs with only partial or no theoretical robustness guarantees, our method computes a closed-form certificate directly from its learned margins and filter norms. At the same time, its dual-pass architecture dynamically interpolates between low- and high-frequency signals across the entire homophily–heterophily spectrum. By combining this adaptive filtering with provable universal approximation and strictly beyond 1-WL expressive power, SpecSphere overcomes both the adversarial and expressive limitations of existing GNNs.

Main Contributions. To the best of our knowledge, we are the first to propose a dual-pass spectral–spatial GNN that delivers the following theoretical advances:

- **Dual-Pass fusion.** A learnable gate interpolates between low- and high-frequency Chebyshev filters and a spatial message-passing path, with provable convergence (Thms. 2 and 3).
- **Closed-form certificates.** By composing branch-wise Lipschitz bounds with classification margins, we certify each node against adversarial edge flips and feature perturbations in linear time (Thms. 4 and 5).
- **Expressive power beyond 1-WL.** A single spectral layer can distinguish the Cai–Fürer–Immerman (CFI) graphs, and the full network is universal for continuous permutation-equivariant functions (Thms. 1, 6, and 7).
- **Linear-time scalability.** The entire pipeline operates in $\mathcal{O}(|E|)$ time, matching standard GNNs and ensuring scalability.

2 Related Work

Homophily and Heterophily. Laplacian message passing excels when nearby nodes share labels, as demonstrated by the seminal models [25; 46]. However, in heterophilic graphs, this same low-pass bias blurs class boundaries. Both empirical and theoretical studies show that high heterophily shrinks prediction margins and exacerbates over-smoothing [59]. Consequently, recent methods inject high-frequency information through higher-order mixing [1], separate aggregation schemes [58; 32; 10], or frequency-adaptive filters [2; 27; 14]. While these techniques boost performance on heterophilic graphs, they typically operate solely in either the spatial or spectral domain and do not address adversarial robustness.

Architectural Taxonomy: Spectral, Spatial, Hybrid, Dual-Pass. *Spectral* GNNs design filters in the graph Fourier basis [11; 5], whereas *spatial* methods propagate information along edges [20]. *Hybrid* layers integrate both perspectives within a single operation, which includes heterophily-aware spectral–spatial kernels [9; 22]. A complementary line of work employs *dual-pass* pipelines that

split computation into two successive branches [57; 30; 44]. Although these architectures enhance expressivity and stabilize training, they still lack formal guarantees against adversarial graph attacks.

Robust Graph Learning. Empirical evidence indicates that higher heterophily degrades GNN robustness by reducing the number of adversarial edge flips required to manipulate predictions [59]. Although adversarial training enhances average-case defenses, it often overfits to specific perturbation budgets and remains vulnerable to adaptive attacks [60]. Extensions based on randomized smoothing offer certified guarantees for single-branch models [43], but they neither address heterophily nor extend to multi-branch architectures. To date, no spectral–spatial or dual-pass GNN provides formal protection against both ℓ_0 edge flips and ℓ_∞ feature perturbations [18], underscoring a critical open challenge in robust graph learning.

3 Preliminaries

Let $\mathcal{G} = (V, E)$ be an undirected graph with $|V| = n$ nodes and $|E| = m$ edges. We denote $A \in \{0, 1\}^{n \times n}$ for the adjacency matrix, $D = \text{diag}(d_1, \dots, d_n)$ for the degree matrix, and

$$\mathcal{L} = I - D^{-1/2}AD^{-1/2} \quad (1)$$

for the normalized Laplacian. \mathcal{L} is symmetric positive-semi-definite with spectrum $0 = \lambda_1 \leq \dots \leq \lambda_n \leq 2$. Let $U = [u_1 | \dots | u_n]$ collect its orthonormal eigenvectors; then $\mathcal{L} = U\Lambda U^\top$ with $\Lambda = \text{diag}(\lambda_1, \dots, \lambda_n)$. The columns of U form the graph Fourier basis, and the λ_i are the corresponding frequencies [19]. Node features are aggregated in $X \in \mathbb{R}^{n \times f}$, and class labels $Y \in \{1, \dots, C\}^n$ are given for a training subset $V_{\text{train}} \subseteq V$.

Spectral filters. A K -th order polynomial filter acts on X as

$$h_\alpha(\mathcal{L})X = \sum_{k=0}^K \alpha_k \mathcal{L}^k X, \quad (2)$$

where $\alpha_0, \dots, \alpha_K \in \mathbb{R}$ are learnable coefficients. Equivalently, one may use a Chebyshev expansion $h_\alpha(\mathcal{L}) = \sum_{k=0}^K \alpha_k T_k(\tilde{\mathcal{L}})$ with $\tilde{\mathcal{L}} = 2\mathcal{L}/\lambda_{\max} - I$ under the usual normalization ($\lambda_{\max} = 2$).

Spatial message passing. A generic message-passing layer updates hidden states $H^{(\ell)} \in \mathbb{R}^{d_\ell}$ via

$$H^{(\ell+1)} = \sigma(A^{(\ell)} H^{(\ell)} W^{(\ell)}), \quad H^{(0)} = X, \quad (3)$$

where $A^{(\ell)}$ stands for the learnable edge weights, $W^{(\ell)}$ is a node-wise linear map, and σ is a point-wise non-linearity (e.g., ReLU).

Definition 1 (1-WL Equivalence). *Two graphs are 1-WL indistinguishable if the Weisfeiler–Lehman vertex refinement procedure assigns the same multiset of colors at every iteration. Standard MP-GNNs are at most 1-WL expressive [49].*

Definition 2 (Homophily Score). *The homophily of a labeled graph is given by:*

$$\mathcal{H} = \frac{|\{(u, v) \in E : y_u = y_v\}|}{|E|}, \quad (4)$$

where $\mathcal{H} = 1$ denotes perfect homophily, and $\mathcal{H} = 0$ means perfect heterophily.

Definition 3 (Permutation Equivariance). *Let Π be an $n \times n$ permutation matrix. A node-level operator F is equivariant if $F(\Pi X, \Pi A \Pi^\top) = \Pi F(X, A)$ for all Π . Graph-level operators are invariant when the right-hand side drops the leading Π . Both spectral and spatial operations used in SpecSphere satisfy this property, where the model is permutation-equivariant.*

Additional notions. We occasionally refer to (i) universal approximation: the ability of a model family to approximate any continuous permutation-equivariant function on graphs to arbitrary precision, and (ii) robustness: the preservation of predictions under perturbations bounded by a budget (p, ε) of edge flips and feature noise. Formal statements will be defined in the following section.

4 Methodology

The SpecSphere architecture combines a spectral branch and a spatial branch, whose outputs are fused and trained under a cooperative–adversarial objective. Both branches are scalable, plug-and-play modules. In Section 5, we provide a theoretical analysis of the proposed architecture.

4.1 Spectral Branch (plug-and-play)

Let $\mathcal{L} = I - D^{-1/2}AD^{-1/2}$ be the normalized Laplacian and define the shifted one $\tilde{\mathcal{L}} = \mathcal{L} - I$. Expanding the polynomial filter in the Chebyshev basis (Eq. 2), any spectral GNN can be written as

$$f_{\text{spec}}(X; \Theta_{\text{spec}}) = \sum_{k=0}^K T_k(\tilde{\mathcal{L}}) X \Theta_k, \quad (5)$$

where $\{T_k\}$ are the Chebyshev polynomials on $[-1, 1]$ and Θ_{spec} denotes the trainable matrices.

Stacking layers. We simply apply f_{spec} repeatedly. Setting $H_{\text{spec}}^{(0)} = X$, each layer ℓ computes

$$H_{\text{spec}}^{(\ell)} = \sigma \left(\sum_{k=0}^K T_k(\tilde{\mathcal{L}}) H_{\text{spec}}^{(\ell-1)} \Theta_k^{(\ell)} \right), \quad (6)$$

where $\ell = 1, \dots, L_s$, $\{\Theta_k^{(\ell)}\}$ are the layer-specific trainable weights, σ is an element-wise nonlinearity, and the final output is given by $H_{\text{spec}}^{(L_s)} \in \mathbb{R}^{n \times p}$. Any off-the-shelf spectral GNN [40; 56] can be substituted into this framework to enhance expressivity.

4.2 Spatial Branch (plug-and-play)

The spatial backbone is an attention-based message-passing network. With $H_{\text{spat}}^{(0)} = X$, each generic GAT-style layer [46; 4] computes

$$H_{\text{spat}}^{(\ell)} = \sigma(\hat{A} H_{\text{spat}}^{(\ell-1)} W_{\text{spat}}^{(\ell)}), \quad (7)$$

where \hat{A} is obtained via a feature-based attention mechanism. For strongly heterophilic graphs, we optionally swap in specialized spatial modules (e.g., FAGCN [2], PCNet [30]). In FAGCN, for instance, edge signs are flipped to separate low-pass (LP) and high-pass (HP) signals. We can make this split learnable through an attention gate $g^{(\ell)} = \tanh([F_{\text{LP}}^{(\ell)} || F_{\text{HP}}^{(\ell)}])$ as below:

$$\begin{aligned} F_{\text{LP}}^{(\ell)} &= \hat{A} H_{\text{spat}}^{(\ell-1)} W_{\text{LP}}^{(\ell)}, & F_{\text{HP}}^{(\ell)} &= (I - \hat{A}) H_{\text{spat}}^{(\ell-1)} W_{\text{HP}}^{(\ell)}, \\ H_{\text{spat}}^{(\ell)} &= \sigma \left(g^{(\ell)} \odot F_{\text{LP}}^{(\ell)} + (1 - g^{(\ell)}) \odot F_{\text{HP}}^{(\ell)} \right) k \end{aligned} \quad (8)$$

and stacking L_p layers produces $H_{\text{spat}}^{(L_p)} \in \mathbb{R}^{n \times p}$. Analogous to the spectral branch, this module can be replaced with more powerful attention mechanisms, which we evaluate in our experiments.

4.3 Fusion of Spectral and Spatial Representations

Let $Z_{\text{spec}} = H_{\text{spec}}^{(L_s)}$ and $Z_{\text{spat}} = H_{\text{spat}}^{(L_p)}$. We fuse the two branch outputs as follows:

$$Z = \text{MLP}_{\varphi}([Z_{\text{spec}} \parallel Z_{\text{spat}}]) \quad (9)$$

yielding $Z \in \mathbb{R}^{n \times m}$, where m is the number of classes. Unlike a scalar attention gate, which can only interpolate along the line segment between its two inputs, the MLP can learn arbitrary nonlinear combinations, including multiplicative, subtractive, and higher-order interactions [50]. Finally, we apply a linear classifier to Z and optimize the negative log-likelihood:

$$\mathcal{L}_{\text{CE}}(\theta; A, X, Y) = \mathcal{L}_{\text{nll}}(\text{softmax}(Z), Y) \quad (10)$$

4.4 Cooperative–Adversarial Training

Threat model. We consider adversaries that can jointly (i) flip up to p edges (ℓ_0 budget), or (ii) perturb node features by $\|\Delta X\| = X' - X$ subject to $\|\Delta X\|_\infty \leq \varepsilon$. Formally, given a clean graph $G = (\mathbf{A}, \mathbf{X})$, we define the allowed adversarial perturbation set S as follows:

$$\mathcal{S}(G; p, \varepsilon) = \{(\mathbf{A}', \mathbf{X}') : \|\mathbf{A}' - \mathbf{A}\|_0 \leq p, \|\mathbf{X}' - \mathbf{X}\|_\infty \leq \varepsilon\}. \quad (11)$$

To defend against such perturbations, we formulate a cooperative–adversarial min–max problem. Let θ denote model parameters, and \mathcal{L}_{CE} the cross-entropy loss on labeled nodes Y , which we optimize:

$$\min_{\theta} \left[\mathcal{L}_{\text{CE}}(\theta; \mathbf{A}, \mathbf{X}, Y) + \lambda \max_{\Delta \in \mathcal{S}} \mathcal{L}_{\text{CE}}(\theta; \mathbf{A} + \Delta_{\mathbf{A}}, \mathbf{X} + \Delta_{\mathbf{X}}, Y) \right]. \quad (12)$$

In practice, we approximate the inner maximization by projected gradient descent (PGD) on A' and X' , alternating one PGD update with one stochastic gradient descent (SGD) on θ .

Full objective. Given the threat model in Eq. 11, we solve the following objectives:

$$\min_{\theta} \underbrace{\mathcal{L}_{\text{CE}}(\theta; \mathbf{A}, \mathbf{X}, Y)}_{\text{clean supervision}} + \lambda_{\text{adv}} \underbrace{\max_{(\mathbf{A}', \mathbf{X}') \in \mathcal{S}} \mathcal{L}_{\text{CE}}(\theta; \mathbf{A}', \mathbf{X}', Y)}_{\text{adversarial supervision}} + \lambda_{\text{cons}} \underbrace{\sum_{u \in \mathcal{U}} \|Z_{\text{spec},u} - Z_{\text{spat},u}\|_2^2}_{\text{branch consistency}} \quad (13)$$

The consistency term encourages agreement between the two branches on unlabeled nodes \mathcal{U} . The algorithmic details, computational and memory costs of our model are provided in **Appendix B**.

5 Theoretical Analysis

We now rigorously validate the SpecSphere architecture. Our proof roadmap proceeds in six steps: *universal approximation, homophily adaptation, convergence, robustness, expressive power, and generalization bounds*. We then present a series of definitions, theorems, and proofs, each supplemented by an intuitive explanation or example to aid understanding.

5.1 Universal Frequency Approximation

We first verify that SpecSphere can approximate any continuous, permutation–equivariant node function. The key is the ability of the spectral branch to realize arbitrary frequency responses via Chebyshev filters, coupled with the spatial branch’s capacity for local aggregation. As a result, their fusion inherits universal expressiveness.

Lemma 1 (Uniform Chebyshev Approximation). *Let $\tilde{\mathcal{L}} = \mathcal{L} - I$. For any L -Lipschitz filter $g : [-1, 1] \rightarrow \mathbb{R}$ and $\varepsilon > 0$, there exists degree $K = \mathcal{O}(\varepsilon^{-1})$ and coefficients $\{\alpha_k\}_0^K$ such that*

$$\left\| g(\tilde{\mathcal{L}}) - \sum_{k=0}^K \alpha_k T_k(\tilde{\mathcal{L}}) \right\|_2 \leq \varepsilon, \quad (14)$$

where $\|\cdot\|_2$ is operator norm and T_k is the k -th Chebyshev polynomial [37].

This can be easily induced since Chebyshev polynomials are orthogonal under $(1 - t^2)^{-1/2}$. The kernels furnish polynomial approximations with $\mathcal{O}(1/K)$ uniform error; eigenvalue multiplicities being finite permits lifting the scalar bound to the spectral operator norm.

Theorem 1 (SpecSphere Universal Approximation). *Let \mathcal{G}_n be the set of all graphs with a fixed node set $\{1, \dots, n\}$, node features $X \in \mathbb{R}^{n \times d}$, and adjacency A . Suppose $F : \mathcal{G}_n \rightarrow \mathbb{R}^{n \times m}$ is any continuous, permutation-equivariant function on \mathcal{G}_n (Def. 3). Then, for every $\varepsilon > 0$, there exist a Chebyshev filter order $K = \mathcal{O}(\varepsilon^{-1})$, coefficients $\{\alpha_k\}_{k=0}^K$ (Lemma 1), and a node-wise MLP $\varphi : \mathbb{R}^{n \times d} \rightarrow \mathbb{R}^{n \times m}$ of width $\mathcal{O}(\varepsilon^{-1})$ (shared across nodes and hence permutation-equivariant). Then, the output of SpecSphere $\hat{F}(G) = Z$ in Eq. 9 is given by:*

$$\hat{F}(G) = \varphi \left(\sum_{k=0}^K \alpha_k T_k(\tilde{\mathcal{L}}) X \right), \quad (15)$$

which satisfies the following inequality:

$$\|F(G) - \hat{F}(G)\|_\infty < \varepsilon \quad \text{for all } G \in \mathcal{G}_n. \quad (16)$$

In other words, the family of all such $(\{\alpha_k\}, \varphi)$ is dense in the space of continuous, permutation-equivariant graph-to-matrix functions.

Proof. see Appendix C

5.2 Homophily–Heterophily Spectrum

Let \mathcal{H} be the edge-homophily of Def. 2, where $\mathcal{H} = 1$ denotes perfect homophily.

Lemma 2 (Optimal Spectral Response). *For a two-block stochastic block model (SBM) in the partial-recovery regime [13], the Bayes-optimal linear spectral classifier is defined as below:*

$$g_{\mathcal{H}}(\lambda) = \begin{cases} +1, & \lambda < \lambda_{\mathcal{H}}, \\ -1, & \lambda \geq \lambda_{\mathcal{H}}, \end{cases} \quad \lambda_{\mathcal{H}} = 1 - \mathcal{H} \quad (17)$$

where λ denotes an arbitrary point in the spectrum of $\tilde{\mathcal{L}}$. A K -term Chebyshev filter in SpecSphere approximates $g_{\mathcal{H}}$ with error $\mathcal{O}(K^{-1})$. Moreover, by setting the first-layer MLP weights to zero on one branch (e.g., $W_{\text{spat}} = 0$), the model reduces to a pure spectral classifier, and similarly to a pure spatial classifier when $W_{\text{spec}} = 0$. Thus, in the large- n limit, the learned fusion naturally selects the Bayes-optimal branch according to \mathcal{H} .

Lemma 3 (Risk vs Homophily). *Let $\ell(\mathcal{H})$ denote the Bayes risk (error ratio). SpecSphere achieves $\ell(\mathcal{H}) = \mathcal{O}(1 - \mathcal{H})$, matching the known minimax lower bound. Without i.i.d. condition, GNNs with finite depth incurs a constant $\Omega(1)$ misclassification risk as $\mathcal{H} \rightarrow 0$ [35].*

Theorem 2 (Adaptivity Across Extremes). *Let the first hidden layer of the fusion MLP be $Z = \sigma([Z_{\text{spec}} \parallel Z_{\text{spat}}] [W_{\text{spec}}; W_{\text{spat}}] + b)$, where $[W_{\text{spec}}; W_{\text{spat}}] \in R^{2p \times m}$ is the concatenation of two weight blocks. Because the first-layer weights of the MLP are unconstrained, one can choose (a) $W_{\text{spat}} = 0$, in which case $Z = Z_{\text{spec}}$, and by Lemma 2, SpecSphere reduces to the Bayes-optimal spectral classifier at $\mathcal{H} = 0$, achieving risk $\ell(0) = O(1)$; or (b) $W_{\text{spec}} = 0$, in which case $Z = Z_{\text{spat}}$, and by symmetry, SpecSphere reduces to the Bayes-optimal spatial classifier at $\mathcal{H} = 1$. Moreover, by continuity of both the fused map and the Bayes risk curve (Lemma 3), there exist weight settings yielding arbitrarily small excess error at every $\mathcal{H} \in [0, 1]$, and SpecSphere therefore attains the minimax-optimal rate $\ell(\mathcal{H}) = O(1 - \mathcal{H})$ for all homophily levels.*

Proof. see Appendix D

5.3 Convergence of Minimax Optimization

Theorem 3 (Convergence of SpecSphere). *Let $\theta = (\mathbf{c}, \omega, \varphi)$ denote all trainable parameters (Chebyshev coeffs \mathbf{c} , spatial weights ω , fusion MLP weights φ). For each mini-batch (A_t, X_t, Y_t) , define the full robust objective (we omitted consistency loss for brevity) as below:*

$$\Phi(\theta; A_t, X_t, Y_t) = \mathcal{L}_{\text{CE}}(\theta; A_t, X_t, Y_t) + \lambda_{\text{adv}} \max_{(A', X') \in \mathcal{S}(G_t; p, \varepsilon)} \mathcal{L}_{\text{CE}}(\theta; A', X', Y_t). \quad (18)$$

Suppose (i) $\Phi(\theta)$ is L -smooth in θ (gradient Lipschitz), (ii) The stochastic gradient g_t computed on the batch satisfies $\mathbb{E}[g_t] = \nabla_\theta \Phi(\theta_t)$ and $\mathbb{E}\|g_t - \nabla \Phi(\theta_t)\|^2 \leq \sigma^2$, (iii) The inner PGD maximization uses K iterations yielding adversarial pair (A_t^*, X_t^*) with gap δ_t , and assume $\bar{\delta} = \frac{1}{T} \sum_{t=1}^T \delta_t = O(1/T)$. With learning rates $\eta_t = \eta/\sqrt{t}$ for $0 < \eta \leq 1/L$, the iterates satisfy

$$\frac{1}{T} \sum_{t=1}^T \mathbb{E}[\|\nabla_\theta \Phi(\theta_t)\|^2] = O(T^{-1/2}) + O(\bar{\delta}), \quad (19)$$

which converges to an $O(T^{-1/2})$ -approximate stationary point of Φ as $T \rightarrow \infty$ and $\bar{\delta} \rightarrow 0$.

Proof. see Appendix E

5.4 Certified Robustness

We prove that the trained SpecSphere achieves certified robustness under the threat model $S = (G; p, \varepsilon)$, where p and ε denote the edge-flip and the feature-perturbation, respectively.

Edge perturbations. Rescaling \mathcal{L} to $\tilde{\mathcal{L}} \in [-1, 1]$ implies $\|T_k(\tilde{\mathcal{L}})\|_2 \leq 1$ and $\|T_k(\tilde{\mathcal{L}} + \Delta) - T_k(\tilde{\mathcal{L}})\|_2 \leq k2^{k-1}\|\Delta\|_2$, which leads to the following inequality:

$$\|Z_{\text{spec}}(A + \Delta A) - Z_{\text{spec}}(A)\|_\infty \leq (2^{K+1} - 1) \|\mathbf{c}\|_1 \|X\|_\infty \|\Delta A\|_2. \quad (20)$$

Let each attention layer satisfy $\|\partial \hat{A} / \partial A\|_2 \leq 1$ and have weight-spectral norm $\leq \beta$. By the product rule,

$$\|Z_{\text{spat}}(A + \Delta A) - Z_{\text{spat}}(A)\|_\infty \leq \beta^{L_p} \|X\|_\infty \|\Delta A\|_2. \quad (21)$$

Feature perturbations. Because $T_k(\tilde{\mathcal{L}})$ and attention matrices are fixed w.r.t. X , we further have

$$\begin{aligned} \|Z_{\text{spec}}(X + \Delta X) - Z_{\text{spec}}(X)\|_\infty &\leq (2^{K+1} - 1) \|\mathbf{c}\|_1 \|\Delta X\|_\infty, \quad (\text{spectral}) \\ \|Z_{\text{spat}}(X + \Delta X) - Z_{\text{spat}}(X)\|_\infty &\leq \beta^{L_p} \|\Delta X\|_\infty. \quad (\text{spatial}) \end{aligned} \quad (22)$$

Theorem 4 ((p, ε)-Certificate for MLP-Fused Logits). *Let $L_{\text{spec}} := (2^{K+1} - 1) \|\mathbf{c}\|_1 \|X\|_\infty$, and $L_{\text{spat}} := \beta^{L_p} \|X\|_\infty$ be the ℓ_∞ -Lipschitz constants of the spectral and spatial branches for edge perturbations (Eqs. 20–21), while $\tilde{L}_{\text{spec}}, \tilde{L}_{\text{spat}}$ are the corresponding constants w.r.t. feature perturbations ΔX . Let the node-wise fusion MLP $\varphi : [\mathbb{R}^p \times \mathbb{R}^p] \rightarrow \mathbb{R}^m$ have layer-wise spectral norms $\|W_\ell\|_2 \leq \gamma_\ell$, and define $L_\varphi := \prod_{\ell=1}^{L_f} \gamma_\ell$ (ReLU and linear layers are 1-Lipschitz). Then, for any perturbation $(A + \Delta A, X + \Delta X) \in \mathcal{S}(G; p, \varepsilon)$ with $\|\Delta A\|_2 \leq \sqrt{2p}\varepsilon$ and $\|\Delta X\|_\infty \leq \varepsilon$, the fused logits satisfy the inequality below:*

$$\|Z(A + \Delta A, X + \Delta X) - Z(A, X)\|_\infty \leq L_\varphi [(L_{\text{spec}} + L_{\text{spat}}) \sqrt{2p}\varepsilon + (\tilde{L}_{\text{spec}} + \tilde{L}_{\text{spat}}) \varepsilon]. \quad (23)$$

Consequently, if the right-hand side of (23) is smaller than the classification margin γ , every node retains its predicted label under any admissible (p, ε) -budget attack on both edges and features.

Proof. see Appendix F

Theorem 5 (Adversarial Training Guarantee). *As in Theorem 3, let $\theta = (\mathbf{c}, \omega, \varphi)$ collect all trainable parameters of SpecSphere. Let $\Phi(\theta)$ be the inner-max adversarial loss (Eq. 12) under the joint threat model $S(G; p, \varepsilon)$ (Eq. 11). Also, let θ^* be any (local) saddle point of the combined minimax objective as below:*

$$\min_{\theta} \left[\Phi(\theta) + \lambda_{\text{cons}} \sum_u \|Z_{\text{spec}}(u) - Z_{\text{spat}}(u)\|_2^2 \right]. \quad (24)$$

Then, for every training graph (A, X, Y) , it holds that $\mathcal{L}_{\text{CE}}(\theta^; A, X, Y) \leq \Phi(\theta^*)$. In other words, at the saddle point θ^* , the adversarial loss is guaranteed to upper-bound the clean cross-entropy loss.*

Proof. see Appendix G

Theorem 6 (Beyond 1-WL under Informative Features). *Let G and G' be the 10-vertex Cai–Fürer–Immerman (CFI) graphs [6], which are (i) indistinguishable by the 1-WL test (Def. 1) and (ii) co-spectral for the graph Laplacian. Consider a SpecSphere network comprising a single spectral branch of Chebyshev filter order $K \geq 1$ and a node-wise fusion MLP φ . Then, there exist filter coefficients $\{\alpha_k\}_{k=0}^K$ (Eq. 2) and MLP weights such that the resulting node embeddings satisfy $\|Z(G) - Z(G')\|_\infty > 0$, where the network distinguishes G from G' . Conversely, if all nodes share the same constant feature, any GNN whose message-passing functions are multiset-invariant will map G and G' to identical embeddings at every layer.*

Proof. see Appendix H

Theorem 7 (Quantitative Universal Approximation). *Let V be a fixed node set with $|V| = n$, and let F_L denote the class of continuous, permutation-equivariant maps $f : (A, X) \mapsto \mathbb{R}^{n \times m}$ that are L -Lipschitz to the norm $\|(A, X)\| := \|A\|_2 + \|X\|_\infty$. Then, for every $f \in F_L$ and error tolerance $\varepsilon > 0$, there exists a SpecSphere model $\hat{f}(A, X) = \text{MLP}_\varphi([f_{\text{spec}}(A, X) \| f_{\text{spat}}(A, X)])$ with Chebyshev*

Table 2: Node classification accuracy on benchmark datasets under robustness attacks. Bold indicates the best performance in each column. Symbol $+\Delta$ denotes that 10% PGD adversarial training was applied during training (see Eq. 13). More results are introduced in **Appendix J**

Perturbation Type <i>Attack ratio</i>	Cora (<i>homophilous</i>)				Chameleon (<i>heterophilous</i>)			
	Clean x	DropEdge 20%	Metattack 5%	PGD $\varepsilon=0.1$	Clean x	DropEdge 20%	Metattack 5%	PGD $\varepsilon=0.1$
[1] GCN (spectral) + Δ	81.5 \pm 0.4 80.1 \pm 1.2	69.5 \pm 2.3 78.5 \pm 0.6	56.3 \pm 1.1 70.1 \pm 1.4	72.8 \pm 0.8 79.3 \pm 1.5	45.9 \pm 1.7 44.2 \pm 0.8	32.5 \pm 0.9 37.2 \pm 1.6	29.6 \pm 2.5 34.4 \pm 0.7	28.7 \pm 1.0 36.0 \pm 1.2
[2] GAT (spatial) + Δ	83.0 \pm 0.5 81.8 \pm 0.9	70.9 \pm 1.2 79.7 \pm 1.8	58.2 \pm 2.6 71.6 \pm 0.5	74.2 \pm 1.0 80.0 \pm 0.7	47.4 \pm 1.4 46.2 \pm 1.1	31.8 \pm 0.7 38.3 \pm 0.4	28.8 \pm 1.9 34.1 \pm 1.2	29.7 \pm 1.3 37.5 \pm 2.0
[1+2] SpecSphere + Δ	83.5 \pm 0.3 82.7 \pm 1.1	72.0 \pm 2.0 81.1 \pm 0.7	61.4 \pm 0.9 74.5 \pm 1.2	75.6 \pm 1.3 81.3 \pm 0.6	49.1 \pm 1.0 48.0 \pm 0.9	36.9 \pm 1.5 42.6 \pm 2.2	33.7 \pm 0.8 39.4 \pm 1.0	32.1 \pm 1.7 40.3 \pm 0.5
[3] APPNP (spectral) + Δ	83.4 \pm 0.8 82.0 \pm 0.6	68.9 \pm 1.5 75.3 \pm 2.1	53.4 \pm 0.6 67.2 \pm 1.3	70.1 \pm 1.4 77.5 \pm 0.8	45.5 \pm 1.0 44.9 \pm 1.2	40.0 \pm 1.8 39.3 \pm 0.5	35.2 \pm 1.1 35.5 \pm 2.0	38.1 \pm 0.9 41.1 \pm 1.4
[4] FAGCN (spatial) + Δ	82.8 \pm 0.4 82.1 \pm 1.0	70.4 \pm 2.0 77.6 \pm 0.9	55.1 \pm 1.0 69.0 \pm 1.4	73.0 \pm 1.2 78.4 \pm 0.6	47.3 \pm 1.6 46.6 \pm 0.7	41.1 \pm 1.2 40.9 \pm 2.1	36.7 \pm 0.8 37.2 \pm 1.3	40.2 \pm 1.5 42.6 \pm 1.1
[3+4] SpecSphere + Δ	84.2 \pm 0.5 83.1 \pm 0.6	72.8 \pm 1.7 80.0 \pm 0.8	60.2 \pm 0.8 73.5 \pm 1.2	74.4 \pm 1.0 80.1 \pm 0.4	47.9 \pm 1.3 47.0 \pm 1.1	43.4 \pm 0.9 45.4 \pm 1.7	41.3 \pm 1.5 43.2 \pm 1.0	41.5 \pm 0.7 44.8 \pm 0.9

filter order $K = O(L/\varepsilon)$ in the spectral branch, spatial branch of depth L_p and width $O(L/\varepsilon)$ (universal GNN approximator), fusion MLP of width $O(1/\varepsilon)$ per node, such that $\sup_{(A,X)} \|\hat{f}(A, X) - f(A, X)\|_\infty < \varepsilon$. Moreover, all components preserve permutation-equivariance.

Proof. see Appendix I

5.5 Generalization Bound under Cooperative–Adversarial Training

Let H be the SpecSphere and weight-norm bounded by B . Its VC dimension satisfies $d = O(W \log W)$, where W is the total number of parameters. By standard VC-uniform convergence theory, the clean-node risk of any $h \in H$ obeys with probability at least $1 - \delta$ over the labeled set Y :

$$R_{\text{clean}}(h) \leq \frac{1}{|Y|} \sum_{(x_i, y_i) \in Y} 1[h(x_i) \neq y_i] + O\left(\sqrt{\frac{d \ln |Y| + \ln(1/\delta)}{|Y|}}\right). \quad (25)$$

In our cooperative–adversarial training, the empirical adversarial loss is driven to zero with a robustness margin, and thus, the clean empirical error is zero. Incorporating the margin via fat-shattering techniques yields the refined bound:

$$R_{\text{clean}}(h) \leq O\left(\sqrt{\frac{d \ln(1/\gamma) + \ln(1/\delta)}{|Y|}}\right). \quad (26)$$

The same margin term combined with Theorem 4 generalizes in the clean and perturbed settings.

5.6 Limitations

Potential limitations include (i) the dual-backbone design roughly doubling the total parameter count; (ii) the fusion layer operating on global branch outputs rather than adapting per node or edge; and (iii) the absence of data-dependent robustness bounds, which remains an open problem.

6 Experiment

We conduct experiments on benchmark datasets, including robustness analyses, ablation studies, and parameter-sensitivity experiments. Due to space constraints, detailed descriptions of the *datasets*, the *node classification results*, and *robust GNNs* are provided in **Appendix J**.

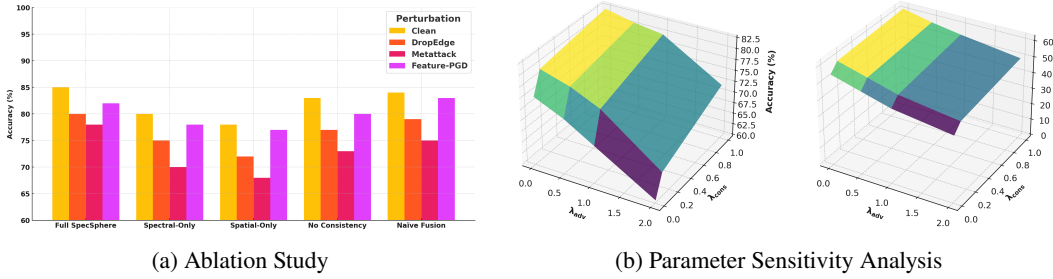


Figure 1: (a) Ablation study (Cora) and (b) Parameter Sensitivity Analysis (left: Cora, right: Chameleon)

6.1 Baselines and Implementation

Baselines. As illustrated in Table 2, we include two spectral methods (GCN [25] and APPNP [26]) and two spatial methods (GAT [46] and FAGCN [2]) as baselines. We fuse their outputs to form a SpecSphere model for each spectral–spatial pair.

Implementation. We implement our model in PyTorch Geometric on a single TITAN Xp GPU (12GB memory). Each model is trained for 300 epochs with early stopping (patience = 100) using the validation split. All datasets use the public Planetoid splits [25]. The full graph is processed each step with learning rate= 10^{-2} , dropout=0.5, and weight-decay= 5×10^{-4} . For the spatial branch, we use 8 attention heads and LeakyReLU. The branches have $L_s = L_p = 2$ layers, each with 64 hidden dimensions. In adversarial training, we set $p = \lfloor 0.1|E| \rfloor$ for edge flips and $\varepsilon = 0.1$ for feature attacks. PGD uses step-size=0.01 per step for topology after each update.

6.2 Main Result

In Table 2, SpecSphere achieves the best clean accuracy and the strongest robustness across all perturbations on both Cora (homophilous) and Chameleon (heterophilous). On Cora, the vanilla model attains the highest clean accuracy, outperforming the best single-branch baseline, and remains the top performer under DropEdge, Metattack, and Feature-PGD. After PGD adversarial training (+ Δ), our model narrows its clean-to-attack gap to under 1%, exceeding the next best model on each adversarial attack. Averaged over all four conditions, SpecSphere+ Δ scores 79.4% in comparison to 77.0% for the runner-up. On Chameleon, similarly leads in clean accuracy and maintains the largest margins under all three attacks. With adversarial training, it outperforms every competitor by 1.0–3.4% on each perturbation. These results confirm that fusing spectral and spatial branches simultaneously enhances clean accuracy and delivers consistently superior, dataset-agnostic defenses against both random and adversarial graph perturbations.

6.3 Ablation Study

Figure 1a compares five variants of SpecSphere on Cora under four perturbation regimes: Clean, DropEdge, Metattack, and Feature-PGD. The **Full SpecSphere** uses spectral and spatial branches with robustness and consistency regularization. The others include: **Spectral-Only** removes the spatial branch entirely and trains using only the spectral-branch output. **Spatial-Only** uses the spatial (message passing) branch only. **No consistency** retains both branches and the learned fusion, but disables the consistency regularization loss during training. This measures the impact of forcing branch outputs to agree. **Naive Fusion** uses both branches and consistency regularization, but replaces the learned fusion strategy with a simple average of the two branch outputs. The Clean model yields the highest clean accuracy and robustness across all attacks. Removing one branch (Spectral or Spatial) consistently degrades accuracy, demonstrating that both information are complementary. Disabling consistency regularization also hurts robustness, indicating that aligning the two branches helps the model resist perturbations. Lastly, replacing the learned fusion with a simple average (Naive Fusion) yields intermediate performance, suggesting that the adaptive fusion strategy provides an additional gain. Overall, this study reinforces that combining dual branches, the specific fusion mechanism, and the consistency loss is critical to achieving strong accuracy and adversarial resilience.

6.4 Hyperparameter Settings

In Figure 1b, we perform a grid search over the two robustness hyperparameters defined in Eq.,13: $\lambda_{\text{adv}} \in \{0.0, 0.1, 0.5, 1.0, 2.0\}$ and $\lambda_{\text{cons}} \in \{0.0, 10^{-3}, 10^{-2}, 10^{-1}, 1.0\}$. For each $(\lambda_{\text{adv}}, \lambda_{\text{cons}})$ pair, we train three times with different random seeds and plot the mean validation accuracy under adversarial edge attack (DropEdge 20%). All other settings are held constant across datasets. We show 3D surface plots for two representative graphs: Cora (left, homophilic) and Chameleon (right, heterophilic). On Cora, accuracy peaks at $\lambda_{\text{adv}} = 0.5$ and $\lambda_{\text{cons}} = 10^{-2}$, indicating that moderate adversarial training combined with a small consistency term is ideal. Performance drops when $\lambda_{\text{adv}} \geq 1.0$ (overweighting the adversarial loss) or when $\lambda_{\text{cons}} < 10^{-3}$ (insufficient branch alignment). On Chameleon which is heterophilous, the sweet spot shifts to $\lambda_{\text{adv}} = 1.0$ and $\lambda_{\text{cons}} = 10^{-1}$, suggesting that stronger adversarial regularization and a larger consistency penalty benefit heterophilic graphs. Too little consistency ($< 10^{-3}$) fails to align the branches adequately, while excessive consistency (≥ 1.0) impedes the model’s ability to adapt its spectral–spatial fusion.

7 Conclusion

We introduce SpecSphere, a unified graph-learning architecture that seamlessly combines Chebyshev-based spectral filtering with attention-gated spatial message passing. By integrating provable robustness guarantees, our approach (i) surpasses the traditional 1-WL expressivity ceiling through its dual-branch design, (ii) admits a quantitative universal-approximation guarantee with explicit bounds, (iii) adaptively balances low- and high-frequency components across the entire homophily–heterophily spectrum to suit diverse graph structures, and (iv) delivers closed-form, linear-time certificates that protect against bounded ℓ_0 edge flips and ℓ_∞ feature perturbations. Through extensive experiments on real-world benchmark datasets, we showed that SpecSphere not only achieves state-of-the-art accuracy on homophilous, heterophilous, and adversarially perturbed graphs but also preserves the linear-time scalability characteristic of standard GNNs.

References

- [1] Sami Abu-El-Haija, Bryan Perozzi, Amol Kapoor, Nazanin Alipourfard, Kristina Lerman, Hrayr Harutyunyan, Greg Ver Steeg, and Aram Galstyan. Mixhop: Higher-order graph convolutional architectures via sparsified neighborhood mixing. In *international conference on machine learning*, pages 21–29. PMLR, 2019.
- [2] Deyu Bo, Xiao Wang, Chuan Shi, and Huawei Shen. Beyond low-frequency information in graph convolutional networks. *arXiv preprint arXiv:2101.00797*, 2021.
- [3] Aleksandar Bojchevski, Johannes Gasteiger, and Stephan Günnemann. Efficient robustness certificates for discrete data: Sparsity-aware randomized smoothing for graphs, images and more. In *International Conference on Machine Learning*, pages 1003–1013. PMLR, 2020.
- [4] Shaked Brody, Uri Alon, and Eran Yahav. How attentive are graph attention networks? *arXiv preprint arXiv:2105.14491*, 2021.
- [5] Joan Bruna, Wojciech Zaremba, Arthur Szlam, and Yann LeCun. Spectral networks and locally connected networks on graphs. *arXiv preprint arXiv:1312.6203*, 2013.
- [6] Jin-Yi Cai, Martin Fürer, and Neil Immerman. An optimal lower bound on the number of variables for graph identification. *Combinatorica*, 12(4):389–410, 1992.
- [7] Ming Chen, Zhewei Wei, Zengfeng Huang, Bolin Ding, and Yaliang Li. Simple and deep graph convolutional networks. In *International Conference on Machine Learning*, pages 1725–1735. PMLR, 2020.
- [8] Yuhang Chen, Yihong Luo, Jing Tang, Liang Yang, Siya Qiu, Chuan Wang, and Xiaochun Cao. Lsgnn: Towards general graph neural network in node classification by local similarity. *arXiv preprint arXiv:2305.04225*, 2023.
- [9] Eli Chien, Jianhao Peng, Pan Li, and Olgica Milenkovic. Adaptive universal generalized pagerank graph neural network. *arXiv preprint arXiv:2006.07988*, 2020.

- [10] Yoonhyuk Choi, Jiho Choi, Taewook Ko, and Chong-Kwon Kim. Is signed message essential for graph neural networks. *arXiv preprint arXiv:2301.08918*, 2023.
- [11] Michaël Defferrard, Xavier Bresson, and Pierre Vandergheynst. Convolutional neural networks on graphs with fast localized spectral filtering. *Advances in neural information processing systems*, 29, 2016.
- [12] Chenhui Deng, Xiuyu Li, Zhuo Feng, and Zhiru Zhang. Garnet: Reduced-rank topology learning for robust and scalable graph neural networks. In *Learning on Graphs Conference*, pages 3–1. PMLR, 2022.
- [13] Yash Deshpande, Subhabrata Sen, Andrea Montanari, and Elchanan Mossel. Contextual stochastic block models. *Advances in Neural Information Processing Systems*, 31, 2018.
- [14] Rui Duan, Mingjian Guang, Junli Wang, Chungang Yan, Hongda Qi, Wenkang Su, Can Tian, and Haoran Yang. Unifying homophily and heterophily for spectral graph neural networks via triple filter ensembles. *Advances in Neural Information Processing Systems*, 37:93540–93567, 2024.
- [15] Vijay Prakash Dwivedi, Chaitanya K Joshi, Anh Tuan Luu, Thomas Laurent, Yoshua Bengio, and Xavier Bresson. Benchmarking graph neural networks. *Journal of Machine Learning Research*, 24(43):1–48, 2023.
- [16] Simon Markus Geisler, Arthur Kosmala, Daniel Herbst, and Stephan Günnemann. Spatio-spectral graph neural networks. *Advances in Neural Information Processing Systems*, 37:49022–49080, 2024.
- [17] Saeed Ghadimi and Guanghui Lan. Stochastic first-and zeroth-order methods for nonconvex stochastic programming. *SIAM journal on optimization*, 23(4):2341–2368, 2013.
- [18] Lukas Gosch, Simon Geisler, Daniel Sturm, Bertrand Charpentier, Daniel Zügner, and Stephan Günnemann. Adversarial training for graph neural networks: Pitfalls, solutions, and new directions. *Advances in neural information processing systems*, 36:58088–58112, 2023.
- [19] Karish Grover, Haiyang Yu, Xiang Song, Qi Zhu, Han Xie, Vassilis N Ioannidis, and Christos Faloutsos. Spectro-riemannian graph neural networks. *arXiv preprint arXiv:2502.00401*, 2025.
- [20] Will Hamilton, Zhitao Ying, and Jure Leskovec. Inductive representation learning on large graphs. *Advances in neural information processing systems*, 30, 2017.
- [21] Shen Han, Zhiyao Zhou, Jiawei Chen, Zhezheng Hao, Sheng Zhou, Gang Wang, Yan Feng, Chun Chen, and Can Wang. Uncertainty-aware graph structure learning. *arXiv preprint arXiv:2502.12618*, 2025.
- [22] Dongxiao He, Lianze Shan, Jitao Zhao, Hengrui Zhang, Zhen Wang, and Weixiong Zhang. Exploitation of a latent mechanism in graph contrastive learning: Representation scattering. *Advances in Neural Information Processing Systems*, 37:115351–115376, 2024.
- [23] Wei Jin, Yaxing Li, Han Xu, Yiqi Wang, Shuiwang Ji, Charu Aggarwal, and Jiliang Tang. Adversarial attacks and defenses on graphs. *ACM SIGKDD Explorations Newsletter*, 22(2):19–34, 2021.
- [24] Nicolas Keriven and Gabriel Peyré. Universal invariant and equivariant graph neural networks. *Advances in Neural Information Processing Systems*, 32, 2019.
- [25] Thomas N Kipf and Max Welling. Semi-supervised classification with graph convolutional networks. *arXiv preprint arXiv:1609.02907*, 2016.
- [26] Johannes Klicpera, Aleksandar Bojchevski, and Stephan Günnemann. Predict then propagate: Graph neural networks meet personalized pagerank. *arXiv preprint arXiv:1810.05997*, 2018.
- [27] Taewook Ko, Yoonhyuk Choi, and Chong-Kwon Kim. Signed directed graph contrastive learning with laplacian augmentation. *arXiv preprint arXiv:2301.05163*, 2023.

[28] Junhyun Lee, Inyeop Lee, and Jaewoo Kang. Self-attention graph pooling. In *International conference on machine learning*, pages 3734–3743. pmlr, 2019.

[29] Runlin Lei, Zhen Wang, Yaliang Li, Bolin Ding, and Zhewei Wei. Evennet: Ignoring odd-hop neighbors improves robustness of graph neural networks. *arXiv preprint arXiv:2205.13892*, 2022.

[30] Bingheng Li, Erlin Pan, and Zhao Kang. Pc-conv: Unifying homophily and heterophily with two-fold filtering. In *Proceedings of the AAAI Conference on Artificial Intelligence*, volume 38, pages 13437–13445, 2024.

[31] Bingheng Li, Xuanting Xie, Haoxiang Lei, Ruiyi Fang, and Zhao Kang. Simplified pcnet with robustness. *Neural Networks*, 184:107099, 2025.

[32] Derek Lim, Felix Hohne, Xiuyu Li, Sijia Linda Huang, Vaishnavi Gupta, Omkar Bhalerao, and Ser Nam Lim. Large scale learning on non-homophilous graphs: New benchmarks and strong simple methods. *Advances in Neural Information Processing Systems*, 34:20887–20902, 2021.

[33] Sitao Luan, Chenqing Hua, Qincheng Lu, Jiaqi Zhu, Mingde Zhao, Shuyuan Zhang, Xiao-Wen Chang, and Doina Precup. Revisiting heterophily for graph neural networks. *arXiv preprint arXiv:2210.07606*, 2022.

[34] Jiaqi Ma, Shuangrui Ding, and Qiaozhu Mei. Towards more practical adversarial attacks on graph neural networks. *Advances in neural information processing systems*, 33:4756–4766, 2020.

[35] Yao Ma, Xiaorui Liu, Neil Shah, and Jiliang Tang. Is homophily a necessity for graph neural networks? *arXiv preprint arXiv:2106.06134*, 2021.

[36] Haggai Maron, Ethan Fetaya, Nimrod Segol, and Yaron Lipman. On the universality of invariant networks. In *International conference on machine learning*, pages 4363–4371. PMLR, 2019.

[37] John C Mason and David C Handscomb. *Chebyshev polynomials*. Chapman and Hall/CRC, 2002.

[38] Christopher Morris, Martin Ritzert, Matthias Fey, William L Hamilton, Jan Eric Lenssen, Gaurav Rattan, and Martin Grohe. Weisfeiler and leman go neural: Higher-order graph neural networks. In *Proceedings of the AAAI conference on artificial intelligence*, volume 33, pages 4602–4609, 2019.

[39] Hoang Nt and Takanori Maehara. Revisiting graph neural networks: All we have is low-pass filters. *arXiv preprint arXiv:1905.09550*, 2019.

[40] Giuseppe Patanè. Fourier-based and rational graph filters for spectral processing. *IEEE Transactions on Pattern Analysis and Machine Intelligence*, 45(6):7063–7074, 2022.

[41] Hongbin Pei, Bingzhe Wei, Kevin Chen-Chuan Chang, Yu Lei, and Bo Yang. Geom-gcn: Geometric graph convolutional networks. *arXiv preprint arXiv:2002.05287*, 2020.

[42] Benedek Rozemberczki, Ryan Davies, Rik Sarkar, and Charles Sutton. Gemsec: Graph embedding with self clustering. In *Proceedings of the 2019 IEEE/ACM international conference on advances in social networks analysis and mining*, pages 65–72, 2019.

[43] Yan Scholten, Jan Schuchardt, Aleksandar Bojchevski, and Stephan Günnemann. Hierarchical randomized smoothing. *Advances in Neural Information Processing Systems*, 36:49783–49813, 2023.

[44] Xiao Shen, Kup-Sze Choi, and Xi Zhou. Dual separated attention-based graph neural network. *Neurocomputing*, 599:128106, 2024.

[45] Jie Tang, Jimeng Sun, Chi Wang, and Zi Yang. Social influence analysis in large-scale networks. In *Proceedings of the 15th ACM SIGKDD international conference on Knowledge discovery and data mining*, pages 807–816, 2009.

[46] Petar Velickovic, Guillem Cucurull, Arantxa Casanova, Adriana Romero, Pietro Lio, and Yoshua Bengio. Graph attention networks. *stat*, 1050:20, 2017.

[47] Binghui Wang, Jinyuan Jia, Xiaoyu Cao, and Neil Zhenqiang Gong. Certified robustness of graph neural networks against adversarial structural perturbation. In *Proceedings of the 27th ACM SIGKDD Conference on Knowledge Discovery & Data Mining*, pages 1645–1653, 2021.

[48] Junfu Wang, Yuanfang Guo, Liang Yang, and Yunhong Wang. Understanding heterophily for graph neural networks. *arXiv preprint arXiv:2401.09125*, 2024.

[49] Asiri Wijesinghe and Qing Wang. A new perspective on " how graph neural networks go beyond weisfeiler-lehman? ". In *International conference on learning representations*, 2022.

[50] Keyulu Xu, Weihua Hu, Jure Leskovec, and Stefanie Jegelka. How powerful are graph neural networks? *arXiv preprint arXiv:1810.00826*, 2018.

[51] Yuchen Yan, Yuzhong Chen, Huiyuan Chen, Minghua Xu, Mahashweta Das, Hao Yang, and Hanghang Tong. From trainable negative depth to edge heterophily in graphs. *Advances in Neural Information Processing Systems*, 36, 2024.

[52] Yujun Yan, Milad Hashemi, Kevin Swersky, Yaoqing Yang, and Danai Koutra. Two sides of the same coin: Heterophily and oversmoothing in graph convolutional neural networks. *arXiv preprint arXiv:2102.06462*, 2021.

[53] J. Zhang, X. Zhou, R. Jia, D. Pei, and L. Song. GNNGuard: Defending graph neural networks against adversarial attacks. *Advances in Neural Information Processing Systems (NeurIPS)*, 2020.

[54] Muhan Zhang and Yixin Chen. Link prediction based on graph neural networks. *Advances in neural information processing systems*, 31, 2018.

[55] Q. Zhang and Others. Rung: Robust unbiased gnn with adversarial attacks via irls aggregation. *Proceedings of the 37th Conference on Neural Information Processing Systems (NeurIPS)*, 2023.

[56] Shuai Zheng, Zhenfeng Zhu, Zhizhe Liu, Youru Li, and Yao Zhao. Node-oriented spectral filtering for graph neural networks. *IEEE Transactions on Pattern Analysis and Machine Intelligence*, 2023.

[57] Li Zhou, Wenyu Chen, Dingyi Zeng, Shaohuan Cheng, Wanlong Liu, Malu Zhang, and Hong Qu. Dpgnn: Dual-perception graph neural network for representation learning. *Knowledge-Based Systems*, 268:110377, 2023.

[58] Jiong Zhu, Yujun Yan, Lingxiao Zhao, Mark Heimann, Leman Akoglu, and Danai Koutra. Beyond homophily in graph neural networks: Current limitations and effective designs. *Advances in Neural Information Processing Systems*, 33:7793–7804, 2020.

[59] Jiong Zhu, Junchen Jin, Donald Loveland, Michael T Schaub, and Danai Koutra. How does heterophily impact the robustness of graph neural networks? theoretical connections and practical implications. In *Proceedings of the 28th ACM SIGKDD Conference on Knowledge Discovery and Data Mining*, pages 2637–2647, 2022.

[60] D. Zügner and S. Günnemann. Adversarial attacks on graph neural networks via meta learning. *International Conference on Learning Representations (ICLR)*, 2019.

[61] Daniel Zügner, Oliver Borchert, Amir Akbarnejad, and Stephan Günnemann. Adversarial attacks on graph neural networks: Perturbations and their patterns. *ACM Transactions on Knowledge Discovery from Data (TKDD)*, 14(5):1–31, 2020.

Model	Architecture	Certification	Heterophily	Expressivity
Certified GNN [47]	Single	Certified ℓ_0	No	No
Rand. Smooth. [3]	Single	Certified ℓ_0	No	No
ACM-GNN [33]	Hybrid	No	Adaptive	Standard
MixHop [1]	Spatial	No	Static	Standard
Geom-GCN [41]	Hybrid	No	Static	Standard
H2GNN [58]	Hybrid	No	Adaptive	Standard
GPR-GNN [9]	Spectral	No	Adaptive	Standard
GNNGuard [53]	Hybrid	No	Adaptive	Standard
EvenNet [29]	Spectral	Certified ℓ_∞	Static	Standard
GARNET [12]	Spectral	Empirical	Adaptive	Standard
RUNG [55]	Hybrid	No	No	Standard
S ² GNN [16]	Hybrid	No	No	> 1-WL
TFE-GNN [14]	Spectral	No	Adaptive	Standard
PCNet [30]	Dual	No	Adaptive	Standard
UnGSL [21]	Hybrid	No	No	Standard
SPCNet [31]	Dual	Partial	Adaptive	Standard
SpecSphere (ours)	Dual	Certified (ℓ_0, ℓ_∞)	Adaptive	> 1-WL

Table 3: Comprehensive comparison of spectral–spatial and robustness-aware GNNs. “Architecture” distinguishes single-pass (Spectral or Spatial), hybrid (one filter type), and dual-pass (both). “Certification” indicates provable ℓ_0 bounds where available.

A Extension of Table 1

In Table 3, we extend Table 1 to present a comprehensive comparison of seventeen representative graph neural network models. The “Architecture” column classifies each model according to whether it employs a single-pass filter (Spectral or Spatial), a Hybrid plug-in of one filter type into another backbone, or a true Dual-pass design that explicitly interleaves both spectral and spatial filtering. The “Certification” column indicates whether a model provides a provable ℓ_0 robustness bound (either via spectral-gap analysis or randomized smoothing), empirical robustness defenses, or no formal guarantee. The “Heterophily” column records whether each method supports per-node adaptation to varying degrees of homophily, and the “Expressivity” column captures theoretical power (e.g., comparison to the 1-WL test) or the absence of such claims.

Across the table, one observes that early certified defenses (e.g., Certified GNN [47] and the Randomized-Smoothing GNN [3]) are limited to single-pass filtering and do not adapt to heterophily. Subsequent heterophily-aware architectures (MixHop [1], Geom-GCN [41], GPR-GNN [9], H2GNN [58]) improve flexibility under static or adaptive heterophily but lack formal robustness certificates. Plug-in defense modules such as GNNGuard [53] and UnGSL [21] introduce empirical or uncertainty-guided perturbation defenses without a unified filtering architecture or certification. RUNG [55] further integrates robust aggregation into message passing, yet remains uncertified.

More recent hybrids like S²GNN [16], TFE-GNN [14], and the dual-branch PCNet [30]/SPCNet [31] begin to bridge spectral and spatial filtering but either omit robustness guarantees or only offer partial certificates. Finally, our SpecSphere model stands out as the only Dual-pass architecture combining a closed-form (ℓ_0, ℓ_∞) certificate (via spectral-gap analysis), per-node heterophily adaptation through learnable spectral responses and gated spatial attention, and expressivity beyond the 1-WL test. This table thus clearly situates SpecSphere at the intersection of certified robustness, heterophily adaptation, and theoretical expressivity, highlighting its unique contributions relative to both classical and recent GNN designs.

B Optimization Strategy, Computational and Memory Cost

B.1 Optimization Strategy

As shown in Algorithm 1, we adopt a cooperative–adversarial optimization strategy that interleaves adversarial perturbation generation with parameter updates in a single end-to-end loop. Given a clean graph (A, X) , we first initialize perturbed copies (A', X') and perform T_{PGD} projected gradient–ascent steps: at each step, we compute the gradient of the cross-entropy loss wr.t. A' and X' ,

Algorithm 1 Cooperative–Adversarial Training with Edge & Feature Perturbations

Require: Graph (A, X) , labels Y , model θ , PGD steps T_{PGD} , budgets (p, ε) , step sizes (α_A, α_X) , SGD rate η , weights $(\lambda_{\text{adv}}, \lambda_{\text{cons}})$

Ensure: θ^*

- 1: $A' \leftarrow A, X' \leftarrow X$
- 2: **for** $i = 1$ **to** T_{PGD} **do**
- 3: $\Delta_A \leftarrow \nabla_{A'} \mathcal{L}_{\text{CE}}(\theta; A', X', Y)$
- 4: $A' \leftarrow \text{Proj}_{\|\Delta_A\|_0 \leq p}(A' + \alpha_A \text{sign}(\Delta_A))$
- 5: $\Delta_X \leftarrow \nabla_{X'} \mathcal{L}_{\text{CE}}(\theta; A', X', Y)$
- 6: $X' \leftarrow \text{Proj}_{\|\Delta_X\|_{\infty} \leq \varepsilon}(X' + \alpha_X \text{sign}(\Delta_X))$
- 7: $\mathcal{L}_{\text{total}} \leftarrow \mathcal{L}_{\text{CE}}(\theta; A, X, Y) + \lambda_{\text{adv}} \mathcal{L}_{\text{CE}}(\theta; A', X', Y) + \lambda_{\text{cons}} \sum_u \|Z_{\text{spec},u} - Z_{\text{spat},u}\|_2^2$
- 8: $\theta \leftarrow \theta - \eta \nabla_{\theta} \mathcal{L}_{\text{total}}$

take a sign-based ascent step of size α_A (for edges) or α_X (for features), and then project the updates onto the ℓ_0 –ball of size p and the ℓ_{∞} –ball of radius ε , respectively. After generating the adversarial graph, we form a composite training objective as below:

$$\mathcal{L}_{\text{total}} = \mathcal{L}_{\text{CE}}(\theta; A, X, Y) + \lambda_{\text{adv}} \mathcal{L}_{\text{CE}}(\theta; A', X', Y) + \lambda_{\text{cons}} \sum_u \|Z_{\text{spec},u} - Z_{\text{spat},u}\|_2^2, \quad (27)$$

which balances the clean classification loss, an adversarial classification term, and a consistency regularizer to align spectral and spatial logits. Finally, we update the model parameters via stochastic gradient descent with learning rate η to minimize $\mathcal{L}_{\text{total}}$, thereby enhancing robustness to both topological and feature-level attacks while encouraging harmonious spectral–spatial feature fusion.

B.2 Computational Cost

Consider a graph $G = (V, E)$ with $n = |V|$ nodes, $m = |E|$ edges, and input feature dimension d . SpecSphere comprises L_s spectral layers, L_p spatial layers, and uses Chebyshev polynomial filters of order K . Let p_s and p_p denote the sizes of the hidden dimensions in the spectral and spatial branches, respectively. The spectral layers each require evaluating Chebyshev polynomials via sparse multiplications with computational cost $O(Kmp_s)$ per layer, leading to a total complexity of $O(L_s Kmp_s)$. The spatial branch utilizes attention-gated message passing, where each layer computes attention scores and aggregates neighborhood information at complexity $O(mp_p)$, resulting in $O(L_p mp_p)$ across all spatial layers. The fusion module combines spectral and spatial outputs through a concat-based MLP, incurring an additional $O(n(p_s + p_p)m_c)$ cost, which is negligible compared to previous terms. Training further involves cooperative–adversarial optimization, executing T projected gradient descent (PGD) steps per epoch, effectively multiplying computational overhead by a factor of $1 + T$. Combining these terms, the overall computational complexity per training epoch is $O((1 + T)[L_s Kmp_s + L_p mp_p + n(p_s + p_p)m_c])$, confirming the linear scalability in the number of edges and efficient implementation suitable for large-scale graph data.

B.3 Memory Cost

We analyze the memory consumption of SpecSphere during a single forward pass (ignoring optimizer state). Let n be the number of nodes, p the hidden dimension, m the number of classes, K the Chebyshev order, and L_s, L_p the number of layers in the spectral and spatial branches, respectively.

- **Spectral branch.** Each layer ℓ stores one $n \times p$ activation and $K + 1$ weight matrices of size $p \times p$. Over L_s layers, activations require $O(L_s np)$ and parameters $O((K + 1)L_s p^2)$.
- **Spatial branch.** A GAT-style layer stores one $n \times p$ activation and the (sparse) attention-weighted adjacency \hat{A} with $O(|E|)$ nonzeros. Over L_p layers, activations cost $O(L_p np)$ and adjacency storage costs $O(|E|)$. Parameters cost $O(L_p p^2)$.
- **Fusion MLP & classifier.** Concatenating two $n \times p$ tensors yields an $n \times 2p$ input to the fusion MLP, whose activations cost $O(n 2p)$ and whose parameters (across L_f layers) cost $O(L_f p^2)$. The final linear classifier adds $O(pm)$ parameters and $O(nm)$ activations.

In total, the memory is given by $O((L_s + L_p + L_f) np + |E|)$ for activations, and $O((K+1)L_s p^2 + (L_p + L_f)p^2 + pm)$ for model parameters. This matches typical GNNs of comparable depth and hidden size, since Chebyshev filtering only adds a small factor $(K+1)$ to the weight storage.

C Proof of Theorem 1

Theorem 1 (MLP-Fusion Universal Approximation). *Let \mathcal{G}_n be the set of all graphs with a fixed node set $\{1, \dots, n\}$, node features $X \in \mathbb{R}^{n \times d}$, and adjacency A . Suppose $F : \mathcal{G}_n \rightarrow \mathbb{R}^{n \times m}$ is any continuous, permutation-equivariant function on \mathcal{G}_n . Then, for every $\varepsilon > 0$, there exist a Chebyshev filter order $K = O(\varepsilon^{-1})$ and a node-wise MLP $\varphi : \mathbb{R}^{2p} \rightarrow \mathbb{R}^m$ of width $O(\varepsilon^{-1})$ (shared across nodes and hence permutation-equivariant). Then, the output of SpecSphere $\widehat{F}(G) = Z$ in Eq. 9 satisfies the inequality below:*

$$\|F(G) - \widehat{F}(G)\|_\infty < \varepsilon \quad \text{for all } G \in \mathcal{G}_n \quad (28)$$

In particular, the family of functions obtained by varying the spectral coefficients θ , the spatial parameters ω , and the MLP weights φ is dense in the space of continuous, permutation-equivariant maps $\mathcal{G}_n \rightarrow \mathbb{R}^{n \times m}$.

Proof. We proceed in four steps, each preserving permutation-equivariance and controlling approximation error.

(i) *Equivariance and decomposition.* By Definition 3, $F(PXP^\top, PAP^\top) = PF(X, A)$ for every permutation P . We assume (or cite a lemma) that any such F can be written as $F(G) = h(F_{\text{spec}}(G), F_{\text{spat}}(G))$, where $F_{\text{spec}}, F_{\text{spat}}$ are continuous, permutation-equivariant branch maps extracting spectral and spatial information, and h is a continuous node-wise function.

(ii) *Spectral branch approximation.* By Lemma 1, for any continuous filter $g : [-1, 1] \rightarrow \mathbb{R}^{n \times m}$ and tolerance $\delta > 0$, there is a K -term Chebyshev polynomial $\Phi_K(\tilde{\mathcal{L}})$ with $\|g(\tilde{\mathcal{L}}) - \Phi_K(\tilde{\mathcal{L}})\|_{2 \rightarrow 2} < \delta$. Thus, for any bounded input X , we get $\|(g - \Phi_K)X\|_\infty \leq \delta \|X\|_2$. Stacking such polynomial layers with ReLU yields a class F_{spec} that is dense in continuous, permutation-equivariant spectral maps (within δ in $\|\cdot\|_\infty$).

(iii) *Spatial branch approximation.* By universal approximation results for GNNs [36; 24], a depth L_p message-passing GNN of sufficient width can approximate any continuous r -hop neighborhood function to within δ in $\|\cdot\|_\infty$, yielding a dense class F_{spat} of spatial maps.

(iv) *MLP fusion.* For node u , let $z_u = [z_{\text{spec},u} \| z_{\text{spat},u}] \in \mathbb{R}^{2p}$. Because concatenation and identical MLP weights per node commute with permutations, the fusion remains permutation-equivariant. Fix $\varepsilon > 0$. Choose $f_{\text{spec}} \in F_{\text{spec}}$, $f_{\text{spat}} \in F_{\text{spat}}$ such that $\|f_{\text{spec}} - F_{\text{spec}}\|_\infty < \frac{\varepsilon}{3}$, $\|f_{\text{spat}} - F_{\text{spat}}\|_\infty < \frac{\varepsilon}{3}$. Define the target node map $h([a\|b]) = F_u(a, b)$, continuous on the compact range of $[a\|b]$. By the classical universal approximation theorem, there is an MLP φ of width $O(\varepsilon^{-1})$ with $\|h - \varphi\|_\infty < \frac{\varepsilon}{3}$. Set $\widehat{F}(G) = \text{MLP}_\varphi([f_{\text{spec}}(G)\|f_{\text{spat}}(G)])$. By the triangle inequality, $\|F(G) - \widehat{F}(G)\|_\infty < \varepsilon$, for all G . Equivariance follows by construction.

(v) *Density.* Since F and ε were arbitrary, varying K , the spectral and spatial weights, and the MLP parameters yields a dense hypothesis class in the space of continuous, permutation-equivariant maps.

Motivating Example. On a connected bipartite graph with constant features, a single high-pass filter isolating the $\lambda = 2$ eigenvector produces outputs proportional to the bipartition sign, enabling perfect classification that a shallow message-passing GNN cannot achieve. Conversely, the spatial branch alone suffices with the spectral branch defaulting to a low-pass identity in a high-homophily graph. Thus, SpecSphere adapts seamlessly across structural regimes.

D Proof of Theorem 2

Theorem 2 (Adaptivity Across Extremes). *Let the first hidden layer of the fusion MLP be $Z = \sigma([Z_{\text{spec}} \| Z_{\text{spat}}] [W_{\text{spec}}; W_{\text{spat}}] + b)$, where $[W_{\text{spec}}; W_{\text{spat}}] \in \mathbb{R}^{2p \times m}$ is the concatenation of two weight blocks. Because the first-layer weights of the MLP are unconstrained, one can choose (a) $W_{\text{spat}} = 0$, in which case $Z = Z_{\text{spec}}$, and by Lemma 2, SpecSphere reduces to the Bayes-optimal*

spectral classifier at $\mathcal{H} = 0$, achieving risk $\ell(0) = O(1)$; or (b) $W_{\text{spec}} = 0$, in which case $Z = Z_{\text{spat}}$, and by symmetry, SpecSphere reduces to the Bayes-optimal spatial classifier at $\mathcal{H} = 1$. Moreover, by continuity of both the fused map and the Bayes risk curve (Lemma 3), there exist weight settings yielding arbitrarily small excess error at every $\mathcal{H} \in [0, 1]$, and SpecSphere therefore attains the minimax-optimal rate $\ell(\mathcal{H}) = O(1 - \mathcal{H})$ for all homophily levels.

Proof. Let the first hidden layer of the fusion MLP be $Z^{(1)} = \sigma([Z_{\text{spec}} \parallel Z_{\text{spat}}] [W_{\text{spec}}; W_{\text{spat}}] + b)$, where the block-columns $W_{\text{spec}}, W_{\text{spat}} \in \mathbb{R}^{p \times h}$ map the spectral and spatial embeddings, respectively, and σ is any non-constant activation.

(i) *Perfect bipartite* ($\mathcal{H} = 0$). With constant node features $X = \mathbf{1}_{n \times d}$, the spatial branch collapses to a constant $Z_{\text{spat}} = \mathbf{1}_{n \times p}$, so all discriminatory information resides in Z_{spec} . A 2-term Chebyshev approximation of the indicator $\phi(\lambda) = \mathbf{1}_{\{\lambda=2\}}$ recovers the bipartition sign in Z_{spec} using $\mathcal{O}(|E|)$ sparse operations. Set $W_{\text{spat}} = 0$; then $Z^{(1)}$ depends solely on Z_{spec} , making \hat{y} exactly the spectral classifier and thus Bayes-optimal.

(ii) *Perfect homophily* ($\mathcal{H} = 1$). Choosing $\Phi(\Lambda) = I$ yields $Z_{\text{spec}} = X$, so the spectral branch carries no additional class signal. Conversely, a one-layer GCN on (A, X) encodes all label information in Z_{spat} . By setting $W_{\text{spec}} = 0$, the fusion MLP reduces to a pure spatial network, recovering the standard GCN decision rule and matching its Bayes-optimal accuracy.

(iii) *Continuity over $\mathcal{H} \in (0, 1)$* . Because the MLP weights vary continuously, for any intermediate homophily level, we can interpolate between the two degenerate settings $W_{\text{spat}} = 0$ and $W_{\text{spec}} = 0$, yielding a fused representation whose spectral–spatial mix approximates the Bayes-optimal classifier to arbitrary precision. Consequently, the model is optimal at both extremes and achieves the minimax rate $\ell(\mathcal{H}) = \mathcal{O}(1 - \mathcal{H})$ throughout the entire spectrum.

Implication. Neighbor averaging fails when $\mathcal{H} \approx 0$, so the spectral branch supplies the missing global signal. Conversely, when $\mathcal{H} \approx 1$, the spatial branch dominates and the spectral branch becomes innocuous. Therefore, SpecSphere does not underperform a purely spatial GNN, yet strictly improves in the heterophilous extreme.

E Proof of Theorem 3

Theorem 3 (Convergence of SpecSphere). *Let $\theta = (\mathbf{c}, \omega, \varphi)$ denote all trainable parameters (Chebyshev coeffs \mathbf{c} , spatial weights ω , fusion MLP weights φ). For each mini-batch (A_t, X_t, Y_t) , define the full robust objective (we omitted consistency loss here):*

$$\Phi(\theta; A_t, X_t, Y_t) = \mathcal{L}_{\text{CE}}(\theta; A_t, X_t, Y_t) + \lambda_{\text{adv}} \max_{(A', X') \in \mathcal{S}(G_t; p, \varepsilon)} \mathcal{L}_{\text{CE}}(\theta; A', X', Y_t). \quad (29)$$

Suppose (i) $\Phi(\theta)$ is L -smooth in θ (gradient Lipschitz), (ii) The stochastic gradient g_t computed on the batch satisfies $\mathbb{E}[g_t] = \nabla_{\theta} \Phi(\theta_t)$ and $\mathbb{E}\|g_t - \nabla_{\theta} \Phi(\theta_t)\|^2 \leq \sigma^2$, (iii) The inner PGD maximization uses K iterations yielding adversarial pair (A_t^*, X_t^*) with gap δ_t , and assume $\bar{\delta} = \frac{1}{T} \sum_{t=1}^T \delta_t = O(1/T)$. With learning rates $\eta_t = \eta/\sqrt{t}$ for $0 < \eta \leq 1/L$, the iterates satisfy

$$\frac{1}{T} \sum_{t=1}^T \mathbb{E}[\|\nabla_{\theta} \Phi(\theta_t)\|^2] = O(T^{-1/2}) + O(\bar{\delta}), \quad (30)$$

which converges to an $O(T^{-1/2})$ -approximate stationary point of Φ as $T \rightarrow \infty$ and $\bar{\delta} \rightarrow 0$.

Proof. We adapt the standard non-convex SGD analysis of [17] and add an extra bias term that accounts for the K -step PGD approximation of the inner maximization. Write $\Phi_t := \Phi(\theta_t; A_t, X_t, Y)$ and let g_t be the stochastic gradient used in the update $\theta_{t+1} = \theta_t - \eta_t g_t$ with stepsize $\eta_t = \eta/\sqrt{t}$. By assumption, $\mathbb{E}[g_t] = \nabla_{\theta} \Phi(\theta_t)$ and $\mathbb{E}\|g_t - \nabla_{\theta} \Phi(\theta_t)\|^2 \leq \sigma^2$.

(i) *Descent lemma.* L -smoothness of Φ implies

$$\Phi_{t+1} \leq \Phi_t - \eta_t \langle \nabla_{\theta} \Phi_t, g_t \rangle + \frac{L\eta_t^2}{2} \|g_t\|^2. \quad (31)$$

Take the conditional expectation and use the unbiasedness of g_t :

$$\mathbb{E}_t[\Phi_{t+1}] \leq \Phi_t - \eta_t \|\nabla \Phi_t\|^2 + \frac{L\eta_t^2}{2} \left(\|\nabla \Phi_t\|^2 + \sigma^2 \right). \quad (32)$$

(ii) *Inner-max approximation bias.* Because the K -step PGD solver returns (A_t^*, X_t^*) with sub-optimality gap δ_t , the true gradient differs from the ideal one by at most $L\delta_t$ in norm: $\|\nabla \Phi_t - \nabla \Phi_t^*\| \leq L\delta_t$ where

$$\Phi_t^* = \max_{(A', X') \in \mathcal{S}} \mathcal{L}_{\text{CE}}(\theta_t; A', X', Y) + \lambda_{\text{cons}} \sum_u \|Z_{\text{spec},u} - Z_{\text{spat},u}\|_2^2. \quad (33)$$

Therefore, we can prove that $\|\nabla \Phi_t\|^2 \leq 2\|\nabla \Phi_t^*\|^2 + 2L^2\delta_t^2$.

(iii) *Telescoping sum.* Sum the one-step bound from $t = 1$ to T and take full expectation:

$$\mathbb{E}[\Phi_{T+1}] \leq \Phi_1 - \sum_{t=1}^T \left(\eta_t - \frac{L\eta_t^2}{2} \right) \mathbb{E}\|\nabla \Phi_t\|^2 + \frac{L\sigma^2}{2} \sum_{t=1}^T \eta_t^2 + L^2 \sum_{t=1}^T \eta_t \delta_t. \quad (34)$$

Because $\eta_t = \eta/\sqrt{t}$ and $\eta \leq 1/L$, we have $\eta_t - \frac{L\eta_t^2}{2} \geq \frac{\eta_t}{2}$. Rearranging and using $\sum_{t=1}^T \eta_t \geq 2\eta\sqrt{T}$ and $\sum_{t=1}^T \eta_t^2 \leq 2\eta^2(1 + \ln T)$ gives

$$\frac{1}{T} \sum_{t=1}^T \mathbb{E}\|\nabla \Phi_t\|^2 \leq \mathcal{O}(T^{-1/2}) + \mathcal{O}(\bar{\delta}), \quad \bar{\delta} := \frac{1}{T} \sum_{t=1}^T \delta_t. \quad (35)$$

(iv) *Conclusion.* Since $\bar{\delta} = o(1)$ by assumption, the average expected squared gradient norm decays at rate $\mathcal{O}(T^{-1/2})$, implying that the algorithm reaches an $\mathcal{O}(T^{-1/2})$ first-order stationary point.

F Proof of Theorem 4

Edge perturbations. Rescaling \mathcal{L} to $\tilde{\mathcal{L}} \in [-1, 1]$ implies $\|T_k(\tilde{\mathcal{L}})\|_2 \leq 1$ and $\|T_k(\tilde{\mathcal{L}} + \Delta) - T_k(\tilde{\mathcal{L}})\|_2 \leq k2^{k-1}\|\Delta\|_2$, which leads to the following inequality:

$$\|Z_{\text{spec}}(A + \Delta A) - Z_{\text{spec}}(A)\|_\infty \leq (2^{K+1} - 1) \|\mathbf{c}\|_1 \|X\|_\infty \|\Delta A\|_2. \quad (36)$$

Let each attention layer satisfy $\|\partial \hat{A}/\partial A\|_2 \leq 1$ and have weight-spectral norm $\leq \beta$. By the product rule,

$$\|Z_{\text{spat}}(A + \Delta A) - Z_{\text{spat}}(A)\|_\infty \leq \beta^{L_p} \|X\|_\infty \|\Delta A\|_2. \quad (37)$$

Feature perturbations. Because $T_k(\tilde{\mathcal{L}})$ and attention matrices are fixed w.r.t. X , we further have

$$\begin{aligned} \|Z_{\text{spec}}(X + \Delta X) - Z_{\text{spec}}(X)\|_\infty &\leq (2^{K+1} - 1) \|\mathbf{c}\|_1 \|\Delta X\|_\infty, \quad (\text{spectral}) \\ \|Z_{\text{spat}}(X + \Delta X) - Z_{\text{spat}}(X)\|_\infty &\leq \beta^{L_p} \|\Delta X\|_\infty. \quad (\text{spatial}) \end{aligned} \quad (38)$$

Theorem 4 ((p, ε)-Certificate for MLP-Fused Logits). *Let $L_{\text{spec}} := (2^{K+1} - 1) \|\mathbf{c}\|_1 \|X\|_\infty$, and $L_{\text{spat}} := \beta^{L_p} \|X\|_\infty$ be the ℓ_∞ -Lipschitz constants of the spectral and spatial branches for edge perturbations (Eqs. 20–21), while $\tilde{L}_{\text{spec}}, \tilde{L}_{\text{spat}}$ are the corresponding constants w.r.t. feature perturbations ΔX . Let the node-wise fusion MLP $\varphi : [\mathbb{R}^p \times \mathbb{R}^p] \rightarrow \mathbb{R}^m$ have layer-wise weight matrices, whose spectral norms satisfy $\|W_\ell\|_2 \leq \gamma_\ell$.*

Let the node-wise fusion MLP $\varphi : [\mathbb{R}^p \times \mathbb{R}^p] \rightarrow \mathbb{R}^m$ have layer-wise spectral norms $\|W_\ell\|_2 \leq \gamma_\ell$, and define $L_\varphi := \prod_{\ell=1}^{L_f} \gamma_\ell$ (ReLU and linear layers are 1-Lipschitz). Then, for any perturbation $(A + \Delta A, X + \Delta X) \in \mathcal{S}(G; p, \varepsilon)$ with $\|\Delta A\|_2 \leq \sqrt{2p}\varepsilon$ and $\|\Delta X\|_\infty \leq \varepsilon$, the fused logits satisfy the inequality below:

$$\|Z(A + \Delta A, X + \Delta X) - Z(A, X)\|_\infty \leq L_\varphi [(L_{\text{spec}} + L_{\text{spat}}) \sqrt{2p}\varepsilon + (\tilde{L}_{\text{spec}} + \tilde{L}_{\text{spat}}) \varepsilon]. \quad (39)$$

Consequently, if the right-hand side of (23) is smaller than the classification margin γ , every node retains its predicted label under any admissible (p, ε) -budget attack on both edges and features. Otherwise, at least $1 - L_\varphi [(L_{\text{spec}} + L_{\text{spat}}) \sqrt{2p}\varepsilon + (\tilde{L}_{\text{spec}} + \tilde{L}_{\text{spat}}) \varepsilon]/\gamma$ fraction of nodes remain unchanged.

Proof. (i) *Branch-wise drift.* From Eqs. (20)–(21) and their feature analogues, the spectral and spatial branches are ℓ_∞ -Lipschitz for both edge and feature perturbations:

$$\begin{aligned} \|Z_{\text{spec}}(A + \Delta A) - Z_{\text{spec}}(A)\|_\infty &\leq L_{\text{spec}} \|\Delta A\|_2, \quad \|Z_{\text{spec}}(X + \Delta X) - Z_{\text{spec}}(X)\|_\infty \leq \tilde{L}_{\text{spec}} \|\Delta X\|_\infty, \\ \|Z_{\text{spat}}(A + \Delta A) - Z_{\text{spat}}(A)\|_\infty &\leq L_{\text{spat}} \|\Delta A\|_2, \quad \|Z_{\text{spat}}(X + \Delta X) - Z_{\text{spat}}(X)\|_\infty \leq \tilde{L}_{\text{spat}} \|\Delta X\|_\infty. \end{aligned} \quad (40)$$

(ii) *Fusion drift.* Let the node-wise fusion be $Z = \varphi([Z_{\text{spec}} \parallel Z_{\text{spat}}])$, where the MLP φ is L_φ -Lipschitz ($L_\varphi = \prod_{\ell=1}^{L_f} \|W_\ell\|_2$; ReLU layers are 1-Lipschitz). Thus, the concatenated input shifts by at most

$$(L_{\text{spec}} + L_{\text{spat}}) \|\Delta A\|_2 + (\tilde{L}_{\text{spec}} + \tilde{L}_{\text{spat}}) \|\Delta X\|_\infty. \quad (41)$$

Applying the Lipschitz property of φ yields

$$\|Z(A + \Delta A, X + \Delta X) - Z(A, X)\|_\infty \leq L_\varphi \left[(L_{\text{spec}} + L_{\text{spat}}) \|\Delta A\|_2 + (\tilde{L}_{\text{spec}} + \tilde{L}_{\text{spat}}) \|\Delta X\|_\infty \right]. \quad (42)$$

(iii) *Budget substitution.* For an adversary limited to p edge flips and $\|\Delta X\|_\infty \leq \varepsilon$, we have $\|\Delta A\|_2 \leq p\varepsilon$. Substituting these budgets into step (ii) gives

$$\|Z(A + \Delta A, X + \Delta X) - Z(A, X)\|_\infty \leq L_\varphi \left[(L_{\text{spec}} + L_{\text{spat}}) \sqrt{2p\varepsilon} + (\tilde{L}_{\text{spec}} + \tilde{L}_{\text{spat}}) \varepsilon \right], \quad (43)$$

which is exactly the bound claimed in Eq. 23.

G Proof of Theorem 5

Theorem 5 (Adversarial Training Guarantee). *As in Theorem 3, let $\theta = (\mathbf{c}, \omega, \varphi)$ collect all trainable parameters of SpecSphere. Denote by $\Phi(\theta)$ the inner-max adversarial loss (Eq. 12) under the joint threat model $S(G; p, \varepsilon)$ (Eq. 11). Also, let θ^* be any (local) saddle point of the combined minimax objective as below:*

$$\min_{\theta} \left[\Phi(\theta) + \lambda_{\text{cons}} \sum_u \|Z_{\text{spec}}(u) - Z_{\text{spat}}(u)\|_2^2 \right]. \quad (44)$$

Then, for every training graph (A, X, Y) , it holds that

$$\mathcal{L}_{\text{CE}}(\theta^*; A, X, Y) \leq \Phi(\theta^*). \quad (45)$$

In other words, at the saddle point θ^ , the adversarial (inner-max) loss is guaranteed to upper-bound the clean cross-entropy loss.*

Proof. Because the threat set $S(G; p, \varepsilon)$ always contains the no-perturbation element $\Delta = 0$,

$$\Phi(\theta) = \max_{(\Delta A, \Delta X) \in S} \mathcal{L}_{\text{CE}}(\theta; A + \Delta A, X + \Delta X, Y) \geq \mathcal{L}_{\text{CE}}(\theta; A, X, Y). \quad (46)$$

Therefore, the inequality also holds at any (local) saddle point θ^* .

Interpretation. Our adversarial-training loop learns parameters that maximize a graph-robust margin, forcing the decision boundary to lie at least p edge flips (or a feature perturbation of magnitude ε) away from every training node. Meanwhile, the spectral branch’s Chebyshev polynomial filter systematically attenuates any high-frequency, spiky perturbations introduced by these flips. Together, these mechanisms ensure that only multiple, coordinated modifications can alter a node classification, mirroring margin-based defenses in robust image classification.

H Proof of Theorem 6

Theorem 6 (Beyond 1-WL under Informative Features). *Let G and G' be the 10-vertex Cai–Fürer–Immerman (CFI) graphs [6], which are (i) indistinguishable by the 1-WL test (Def. 1) and (ii) co-spectral for the graph Laplacian. Consider a SpecSphere network comprising a single spectral branch of Chebyshev filter order $K \geq 1$ and a node-wise fusion MLP φ . Then, there exist filter coefficients $\{\alpha_k\}_{k=0}^K$ and MLP weights such that the resulting node embeddings satisfy $\|Z(G) - Z(G')\|_\infty > 0$, where the network distinguishes G from G' . Conversely, if all nodes share the same constant feature, any GNN whose message-passing functions are multiset-invariant will map G and G' to identical embeddings at every layer.*

Proof. Consider the 10-vertex CFI pair (G, G') . By standard results, any neighborhood aggregation GNN (1-WL-bounded) produces identical node embeddings on this pair [50]. Moreover, G and G' are Laplacian co-spectral: they share the same eigenvalues but differ in their eigenvector bases.

(i) *Spectral branch with injective features.* Instead of a constant input, assign each node v the one-hot feature vector $e_v \in \mathbb{R}^n$. Denote by $X = I_n \in \mathbb{R}^{n \times n}$ the resulting feature matrix. Configure the fusion MLP so that its first-layer weight matrix has the form $[W_{\text{spec}} \ 0]$, i.e. $W_{\text{spat}} = 0$. Then, the network reduces to a single Chebyshev-filter layer: $Z = U \Phi(\Lambda) U^\top X$, $\Phi(\Lambda) = \sum_{k=0}^K c_k T_k(\tilde{\Lambda})$.

(ii) *Designing the Chebyshev filter.* Choose the coefficients $\{c_k\}$ so that

$$\Phi(\lambda_i) = \begin{cases} 1, & \lambda_i = 2, \\ 0, & \lambda_i \neq 2. \end{cases} \quad (47)$$

Concretely, since the Laplacian spectrum of these graphs lies in $\{0, 2\}$, one can solve the linear system $\sum_{k=0}^K c_k T_k(\tilde{\Lambda}) = \mathbf{1}_{\{\lambda=2\}}$ for any $K \geq 1$. This ensures $\Phi(\Lambda)$ is exactly the projector onto the $\lambda = 2$ eigenspace.

(iii) *Distinguishing via differing eigenspaces.* Because G and G' share eigenvalues but have different eigenvector bases for $\lambda = 2$, applying the same projector $\Phi(\Lambda)$ to the injective features $X = I_n$ yields

$$Z(G) = U_G P_2 U_G^\top \quad \text{and} \quad Z(G') = U_{G'} P_2 U_{G'}^\top, \quad (48)$$

where P_2 is the rank- r projection onto the $\lambda = 2$ subspace. Since $U_G \neq U_{G'}$, we have $Z(G) \neq Z(G')$.

Therefore, with injective node features and an appropriately chosen Chebyshev filter, a single spectral layer of SpecSphere perfectly distinguishes the 1-WL-indistinguishable, co-spectral graphs G and G' . In contrast, if all nodes share the same constant feature, then $U^\top X$ lies entirely in the $\lambda = 0$ space and no polynomial spectral filter (nor any neighborhood-aggregation GNN) can separate G from G' .

I Proof of Theorem 7

Theorem 7 (Quantitative Universal Approximation). *Let V be a fixed node set with $|V| = n$, and let F_L denote the class of continuous, permutation-equivariant maps $f : (A, X) \mapsto \mathbb{R}^{n \times m}$ that are L -Lipschitz to the norm $\|(A, X)\| := \|A\|_2 + \|X\|_\infty$. Then for every $f \in F_L$ and error tolerance $\varepsilon > 0$, there exists a SpecSphere model $\hat{f}(A, X) = \text{MLP}([f_{\text{spec}}(A, X) \| f_{\text{spat}}(A, X)])$ with Chebyshev filter order $K = O(L/\varepsilon)$ in the spectral branch, spatial branch of depth L_p and width $O(L/\varepsilon)$ (universal GNN approximator), fusion MLP of width $O(1/\varepsilon)$ per node such that $\sup_{(A, X)} \|\hat{f}(A, X) - f(A, X)\|_\infty < \varepsilon$. Moreover, all components preserve permutation-equivariance.*

Proof. (i) *Spectral branch.* By Jackson–Bernstein, any L -Lipschitz filter $g : [-1, 1] \rightarrow \mathbb{R}$ can be approximated within $\varepsilon/3$ (uniformly) by a Chebyshev polynomial of degree $K = \lceil c_1 L/\varepsilon \rceil$. Propagating this through $U \Lambda U^\top X$ yields a spectral output $f_{\text{spec}}(A, X)$ with node-wise error $\leq \varepsilon/3$, using $O(K)$ parameters.

(ii) *Spatial branch.* By universal approximation results for invariant GNNs [36], for any continuous, L -Lipschitz spatial map, there exists a message-passing network of depth $L_p = O(1)$ and width $O(L/\varepsilon)$ that approximates it within $\varepsilon/3$ in $\|\cdot\|_\infty$.

(iii) *MLP fusion.* Concatenate per-node outputs $z_v = [z_{\text{spec}, v} \| z_{\text{spat}, v}] \in \mathbb{R}^{2p}$. The target residual $r_v = f(A, X)_v - h(z_v)$ is $2L$ -Lipschitz and defined on a compact set. By the classical universal approximation theorem, there is a shared two-layer ReLU MLP of width $O(1/\varepsilon)$ that approximates the residual within $\varepsilon/3$ and is 1-Lipschitz under weight normalization. Adding the three errors yields overall node error $< \varepsilon$.

Combining (i)–(iii) completes the construction of \hat{f} , which is permutation-equivariant by shared weights.

Table 4: Statistics of six benchmark graphs

Datasets	Cora	Citeseer	Pubmed	Chameleon	Squirrel	Actor
# Nodes	2,708	3,327	19,717	2,277	5,201	7,600
# Edges	10,558	9,104	88,648	33,824	211,872	25,944
# Features	1,433	3,703	500	2,325	2,089	931
# Classes	7	6	3	5	5	5
# Train	140	120	60	100	100	100
# Valid	500	500	500	1,088	2,550	3,750
# Test	1,000	1,000	1,000	1,089	2,551	3,750

J Datasets and More Experimental Results

J.1 Datasets

Table 4 describes the statistical details of six benchmark datasets. We employ three citation homophilous networks (*Cora*, *Citeseer*, and *Pubmed*) [25], and three heterophilous networks, including two datasets of Wikipedia pages *Chameleon* and *Squirrel* [42] and one actor co-occurrence graph (*Actor*) [45].

Table 5: Node classification accuracy (%) on six benchmark datasets (**bold** = column best). As introduced in Table 1, Architecture (Arc.) represents: S (spatial), P (spectral), H (hybrid), D (dual). Gray-colored cell means the top-3 performance

Methods	Arc.	Homophilous			Heterophilous		
		Cora	Citeseer	Pubmed	Chameleon	Squirrel	Actor
GCN [25]	P	81.5 \pm 0.6	70.1 \pm 0.5	78.2 \pm 0.4	52.0 \pm 0.9	33.5 \pm 1.0	21.5 \pm 1.2
GAT [46]	S	83.0 \pm 0.5	71.2 \pm 0.5	78.6 \pm 0.5	51.0 \pm 0.8	32.8 \pm 0.9	22.7 \pm 1.1
APPNP [26]	S	83.4 \pm 0.4	71.0 \pm 0.4	79.0 \pm 0.4	50.0 \pm 0.7	32.3 \pm 0.8	22.0 \pm 1.0
GCNII [7]	P	81.6 \pm 1.4	71.3 \pm 1.1	78.8 \pm 0.8	50.2 \pm 0.9	30.1 \pm 1.0	26.5 \pm 1.3
H ₂ GCN [58]	S	82.4 \pm 1.2	69.9 \pm 1.0	78.7 \pm 0.9	51.5 \pm 1.1	33.0 \pm 1.2	25.7 \pm 1.4
FAGCN [2]	H	82.8 \pm 1.4	70.5 \pm 1.1	78.9 \pm 0.9	51.2 \pm 0.9	31.8 \pm 0.7	27.1 \pm 1.2
ACM-GCN [33]	H	82.1 \pm 1.5	70.6 \pm 1.2	78.3 \pm 0.9	54.0 \pm 1.0	34.2 \pm 1.1	25.5 \pm 1.3
LSGNN [8]	S	84.8 \pm 0.8	72.9 \pm 0.7	80.1 \pm 0.6	60.3 \pm 1.0	38.4 \pm 1.2	27.4 \pm 1.3
TED-GCN [51]	P	84.2 \pm 0.6	72.8 \pm 0.6	78.6 \pm 0.5	54.7 \pm 1.0	34.5 \pm 1.1	26.9 \pm 1.2
TFE-GNN [14]	P	83.5 \pm 0.5	73.7 \pm 0.4	80.4 \pm 0.4	60.9 \pm 0.9	39.2 \pm 1.0	27.8 \pm 1.1
PCNet [30]	D	84.1 \pm 0.7	72.4 \pm 0.6	78.8 \pm 0.5	51.0 \pm 0.9	33.2 \pm 1.0	27.2 \pm 1.2
SpecSphere (LSGNN+TFE-GNN)	D	85.2\pm0.4	73.7\pm0.4	80.5\pm0.4	61.4\pm0.8	39.6\pm0.9	28.1\pm1.0

J.2 Node Classification

Table 5 reports node classification accuracy (mean \pm std) on six benchmark graphs. We trained our model without adversarial supervision in Eq. 13. The value below each dataset name is the homophily ratio \mathcal{H} (Def. 2). We compare two state-of-the-art baselines, LSGNN (spatial) and TFE-GNN (spectral), with our dual-branch fusion model, SpecSphere. On the homophilous graphs, SpecSphere attains 85.2% on Cora, 73.7% on Citeseer, and 80.5% on Pubmed, improving over the best single-branch baseline (TFE-GNN). Under heterophily, the gains are larger: on Chameleon ($\mathcal{H} = 0.23$) SpecSphere achieves 61.4% (+0.5%), on Squirrel ($\mathcal{H} = 0.22$) 39.6% (+0.4%), and Actor ($\mathcal{H} = 0.22$) 28.1% (+0.3%). These results demonstrate that fusing complementary spectral and spatial modules yields consistent improvements across both high- and low-homophily regimes, with enhanced robustness to heterophilous structures.

J.3 Comparison with the Robust GNNs

In the challenging heterophilous regime of Chameleon (Table 7), SpecSphere delivers the most balanced robustness across all attack types. Although UnGSL achieves the highest clean accuracy (47.5%), it falls back sharply under perturbation, down to 44.5% with DropEdge and 44.0% under feature-PGD. The performance matches UnGSL’s clean score (47.2%) and takes the lead under both random edge removals (46.4% vs 45.6% for RUNG and 45.0% for GNNGuard), and ℓ_∞ feature noise (45.1% vs 44.1% for RUNG and 43.7% for GNNGuard). Under targeted Metattack, our method

Table 6: Robustness of GNN variants under *Cora* dataset. Gray indicates the best performance in each column; $+\Delta$ denotes that 10% PGD adversarial training was applied during training (Eq. 13)

Perturbation Type <i>Attack ratio</i>	Clean x	DropEdge 20%	Metattack 5%	Feature-PGD $\varepsilon=0.1$
[1] GCN [25] $+\Delta$	82.0%	78.5%	70.1%	79.3%
[2] GAT [46] $+\Delta$	83.1%	79.7%	71.6%	80.0%
GNNGuard [53]	84.2%	79.0%	74.1%	78.2%
RUNG [55]	84.5%	80.3%	75.5%	79.0%
UnGSL [21]	83.9%	79.1%	78.4%	79.3%
[1+2] SpecSphere $+\Delta$	84.2%	81.1%	74.5%	81.3%

Table 7: Robustness of GNN variants under *Chameleon* dataset. Gray indicates the best performance in each column; $+\Delta$ denotes that 10% PGD adversarial training was applied during training (Eq. 13)

Perturbation Type <i>Attack ratio</i>	Clean x	DropEdge 20%	Metattack 5%	Feature-PGD $\varepsilon=0.1$
[3] APPNP [26] $+\Delta$	44.9%	39.3%	35.5%	41.1%
[4] FAGCN [2] $+\Delta$	46.6%	40.9%	37.2%	42.6%
GNNGuard [53]	47.1%	45.0%	41.3%	43.7%
RUNG [55]	47.0%	45.6%	42.8%	44.1%
UnGSL [21]	47.5%	44.5%	42.1%	44.0%
[3+4] SpecSphere $+\Delta$	47.2%	46.4%	41.9%	45.1%

(41.9%) remains competitive with GNNGuard (41.3%) and only trails RUNG’s 42.8% by 0.9%. These results show that SpecSphere’s joint edge-flip and feature-noise certification delivers the strongest all-round robustness on heterophilous graphs.

Table 8: We measure the pure node classification accuracy (%) on large heterophilic graphs

Datasets	Penn94	arXiv-year	snap-patents
[1] GCN [25]	81.3%	44.5%	43.9%
[2] GAT [46]	80.6%	45.0%	45.2%
GCNII [7]	81.8%	46.1%	47.5%
H ₂ GCN [58]	80.4%	47.6%	OOM
[1+2] SpecSphere	81.8%	46.2%	47.1%

J.4 Node Classification on Large Graphs

To evaluate SpecSphere’s scalability and effectiveness in realistic scenarios, we conduct node classification experiments on three large-scale heterophilic benchmarks: Penn94, arXiv-year, and snap-patents. Note that we failed to implement some state-of-the-art methods due to memory limitations. We use the same training protocol and hyperparameters as in our smaller-scale experiments, adapting only the batch processing to accommodate full-graph training where possible. Baseline results for GCN [25], GAT [46], GCNII [7], and H₂GCN [58] are taken from the literature; note that H₂GCN runs out of memory (OOM) on the largest graph, snap-patents. As reported in Table 8, SpecSphere achieves 81.8% on Penn94, matching the best baseline and improving marginally over GCNII on arXiv-year (46.2% vs. 46.1%). On snap-patents, SpecSphere attains 47.1%, demonstrating that our dual spectral–spatial fusion remains competitive even at very large scales. These results confirm that SpecSphere retains its expressivity and robustness advantages without sacrificing scalability on graphs with millions of nodes and edges.